Mathematical Biosciences and Engineering

http://www.aimspress.com/journal/mbe

MBE, 21(5): 5900–5946.
DOI: 10.3934/mbe.2024261
Received: 14 February 2024
Revised: 08 April 2024
Accepted: 22 April 2024
Published: 15 May 2024

Research article

The role of immune cells in resistance to oncolytic viral therapy

Prathibha Ambegoda[1], Hsiu-Chuan Wei[2] and Sophia R-J Jang[1,*]

[1] Department of Mathematics & Statistics, Texas Tech University, Lubbock, TX, USA

[2] Department of Applied Mathematics, Feng Chia University, Taichung, Taiwan

* **Correspondence:** Email: sophia.jang@ttu.edu; Tel: +18068347006; Fax: +18067421112.

Abstract: Resistance to treatment poses a major challenge for cancer therapy, and oncoviral treatment encounters the issue of viral resistance as well. In this investigation, we introduce deterministic differential equation models to explore the effect of resistance on oncolytic viral therapy. Specifically, we classify tumor cells into resistant, sensitive, or infected with respect to oncolytic viruses for our analysis. Immune cells can eliminate both tumor cells and viruses. Our research shows that the introduction of immune cells into the tumor-virus interaction prevents all tumor cells from becoming resistant in the absence of conversion from resistance to sensitivity, given that the proliferation rate of immune cells exceeds their death rate. The inclusion of immune cells leads to an additional virus-free equilibrium when the immune cell recruitment rate is sufficiently high. The total tumor burden at this virus-free equilibrium is smaller than that at the virus-free and immune-free equilibrium. Therefore, immune cells are capable of reducing the tumor load under the condition of sufficient immune strength. Numerical investigations reveal that the virus transmission rate and parameters related to the immune response significantly impact treatment outcomes. However, monotherapy alone is insufficient for eradicating tumor cells, necessitating the implementation of additional therapies. Further numerical simulation shows that combination therapy with chimeric antigen receptor (CAR T-cell) therapy can enhance the success of treatment.

Keywords: oncolytic viral therapy; resistance; effector cells; hopf bifurcation

1. Introduction

Malignant tumors, recognized as one of the most lethal diseases globally, arise from uncontrolled cell growth [1,2]. Traditional treatment approaches encompass surgery, chemotherapy, and radiotherapy. An emerging strategy in the field is cancer immunotherapy, a therapeutic approach that entails stimulating and leveraging the immune system to combat the cancer [3].

Certain viruses possess the remarkable ability to precisely select and invade cancer cells while

leaving normal cells unharmed. These specialized viruses are referred to as oncolytic viruses (OVs) and are pivotal in oncoviral therapy (OVT). OVT has demonstrated significant anti-tumor effects in diverse mouse models and clinical studies [3]. Apart from their oncolytic potential to direct towards cancer cells and destroy them, OVs can be engineered to incorporate specific genes or cytokines, enhancing their ability to activate T cell responses [3].

Cancer therapies encounter several formidable challenges, with drug resistance emerging as a major concern. Drug resistance is a frequent outcome in cancer treatment and is categorized as acquired or primary (inherent) resistance. Inherent resistance is intrinsic, whereas acquired resistance develops after exposure to drugs. In [4], Noll et al. presented significant confirmation of inherent resistance in the measles vaccine virus (MeV) against NCI-60 solid cancer cells. The authors concluded that inherent resistance in oncolytic viral therapy may be linked with epigenetic and genetic alterations following malignant transition.

While several computational and mathematical models have been devised to investigate chemotherapy resistance [5–10], there has been relatively less exploration of models focused on other therapeutic resistances. Notably, studies such as [10, 11] delve into acquired/primary resistance in targeted therapy, while [12] utilizes spatial probabilistic models to investigate resistance in oncolytic virotherapy. In their investigation, Bhatt et al. [12] developed probabilistic, cell-based models to explore the dynamics of resistance in OVT. The model encompasses four distinct populations: normal healthy cells, infected cells, infection-sensitive cancer cells, and infection-resistant cancer cells. The authors systematically explored the model's outcomes, analyzing their dependence on various parameter values and assumptions. Key aspects investigated include the impact of the ratio of the death rate of infected cells to the viral spread rate on cancer eradication, the influence of the timing of virotherapy, and the effects of parameters such as the production rate of resistant cancer cells, virus diffusion distance, and the probability of virus infection.

The study [12] utilized simulations based on three different types of cell-based models: 2D lattice, 3D lattice, and Voronoi, demonstrating that the results exhibit qualitative similarity with some variations. Furthermore, the authors examined the scenario of allowing normal healthy cells to become infected. They found that while this approach may increase the likelihood of complete cancer elimination, representing a successful outcome, it comes with the risk of elevating the population of resistant cancer cells, potentially leading to therapy failure. The study suggests that improved therapeutic efficacy can be achieved by sensitizing healthy normal cells to infection [12].

Despite being relatively unexplored, resistance to OVT significantly limits therapeutic effectiveness. The article [13] extensively explores a spectrum of mechanisms contributing to resistance in OVT, shedding light on the multifaceted challenges faced in utilizing viruses as therapeutic agents against cancer. For example, interferon-mediated resistance stands out as a formidable obstacle, as host cells activate interferon pathways to establish an anti-viral state. In addition, epigenetic modifications, encompassing changes in DNA methylation and histone modifications, have been implicated in altering the gene expression landscape, potentially limiting the permissiveness of host cells to oncolytic viruses. The hypoxic microenvironment within tumors presents another layer of complexity, with low oxygen concentrations inhibiting viral replication. Furthermore, virus-entry barriers pose challenges by hindering efficient entry into target cells, while spatiotemporal restrictions to viral spread highlight the intricate dynamics within tumors that may limit the uniform distribution of therapeutic viruses. These identified mechanisms underscore the need for a nuanced understanding to develop strategies that can

effectively overcome OVT resistance and enhance the therapeutic potential of oncolytic viral therapies in the realm of cancer treatment.

The viral cycle in oncolytic viral therapy typically consists of several stages, including attachment and entry, uncoating and gene expression, and replication and assembly [14]. Once the virus attaches to specific receptors on the surface of cancer cells, it enters the cancer cell, either through the cell membrane or via receptor-mediated endocytosis. Inside the cancer cell, the viral genome is released from its protein coat. The virus then utilizes the cellular machinery to express its genes. The viral genome is replicated, and new viral components are synthesized within the host cell. The components are assembled to form new viral particles. These processes take time to complete [14].

To our knowledge, the study [15] represents a pioneering use of deterministic models to explore OVT resistance, although it adopts a generic approach without considering specific mechanisms of resistance. In [15], the authors developed systems of differential equations to study the effects of OVT resistance, with the time delay associated with the infection process. The research presented conditions for the existence of equilibria and their stability, deriving critical delays for Hopf bifurcations. The Hopf bifurcation marks the point at which a stable equilibrium in the model becomes unstable, leading to the emergence of periodic oscillations. This can correspond to the transition from steady tumor growth to oscillatory tumor dynamics, where tumor size fluctuates over time. Understanding the occurrence of Hopf bifurcation in cancer models can provide insights into how tumors respond to different treatment strategies.

The study [15] concluded that if tumor cells resistant to treatment cannot revert naturally to sensitive cells or through other mechanisms, every cancer cell will inevitably develop resistance to the OVT, even when a time delay in the viral infection is present. Additionally, the authors proved that the delay in infection process cannot destabilize those equilibria with no viruses. The numerical investigations conducted by the authors showed that the existence of resistant cancer cells, along with time delay in the virus infection, substantially amplifies the number of tumor cells, particularly during periods of instability in the population interaction, i.e., when the interaction is not at equilibrium.

The immune system, a complex network of organs, cells, and proteins, serves as the body's defense against infections [1]. Malignant tumors often express antigens that can trigger an immune response, creating an anti-tumor effect [1, 2]. According to the Tumor Immuno-Surveillance Hypothesis, the immune system can potentially inhibit the growth of small tumors, eliminating them before they become clinically evident [1, 2]. Building upon the work in [15], this study introduces effector cells into the tumor-virus interaction. These immune cells, activated by tumor cells [16–18], have the ability to eliminate both tumor cells and viruses in oncolytic viral therapy. The primary objective is to investigate the impact of immune cells on the dynamics of the tumor-virus interaction. In addition, as the immune activation process in response to the presence of the tumor is not instantaneous, we introduce a time delay in the activation of immune cells. This results in a model formulated as delay differential equations (DDEs). In contrast to [15], where delay is incorporated into the viral cycle, this study considers a delay in immune activation, as it takes days or even weeks for the adaptive immune response to become established. We derive critical delays for which Hopf bifurcations occur at certain boundary equilibria, where one or more populations become extinct.

Contrary to the findings in [15], the introduction of immune cells in the tumor-virus interaction prevents all tumor cells from becoming resistant when there is no conversion from resistance to sensitivity, provided that the proliferation rate of immune cells exceeds their death rate. However, if

the immune cells have a smaller recruitment rate, then eventually all tumor cells will become resistant. In [15], the model exhibits a unique positive equilibrium, whereas the model with the addition of immune cells into the interaction may have three positive equilibria. This new phenomenon can lead to a more complex interaction. Additionally, the numerical simulations conducted in this study demonstrate that the inclusion of immune cells significantly reduces the total tumor count in both stable and unstable scenarios compared to the results presented in [15]. Furthermore, this study includes global sensitivity analysis and numerical bifurcation analysis. In particular, combined therapies of OVT and CAR T-cell therapy are considered in Section 5.

The subsequent sections unfold as follows: model development is presented in Section 2, followed by the analysis of ordinary differential equations and DDE models in Sections 3 and 4, respectively. Section 5 delves into the numerical investigation, and the final section concludes with a brief discussion. Appendixes A and B discuss the models of special cases, while Appendix C presents the proofs of some analytical results.

2. Model formulation

Cancer cells are categorized as either infected or uninfected. The uninfected tumor cells are further separated into resistant or sensitive to OVT. Let T_r and T_s denote the numbers of uninfected resistant and sensitive cancer cells, respectively. The variable T_i denotes the class of infected tumor cells, and V represents the compartment of free viruses. The number of immune cells at the tumor site is denoted by Z. A non-sensitive cancer cell will produce resistant descendants except if it transforms into sensitivity before birth occurs. We assume that the resistant and sensitive tumor cells have logistic growth with intrinsic growth rates r_r and r_s, respectively, and a carrying capacity denoted by K. While resistant and sensitive tumor cells may differ in their response to oncolytic viral therapy, they still share the same physical environment within the tumor. This environment provides the necessary resources for cell growth and imposes limitations on cell proliferation. Therefore, both types of tumor cells are subject to the same constraints imposed by factors such as nutrient availability and spatial limitations, and consequently, they have the same carrying capacity.

Several researchers propose that non-sensitive cancer cells exhibit a smaller growth rate in comparison to cancer cells that are not resistant due to the associated costs of resistance [5, 12]. To incorporate this finding, we will assume $r_r < r_s$ in numerical simulations. The rate of mutation from sensitivity to resistance is represented by the parameter a. Because infected cancer cells have a short life duration and do not require substantial materials, their geographical occupancy, proliferation, and nutrient absorption are not considered. Refer to [19, 20], in which the tumor's carrying capacity does not include infected cancer cells.

Immune cells are capable of killing sensitive, resistant, and infected tumor cells. Regarding the killing of viruses, it typically involves a separate immune response, such as the innate immune response mediated by phagocytes and the adaptive immune response mediated by antibodies and cytotoxic T cells [21]. The immune cells considered in the model include both innate and adaptive systems, where the immune cells are not activated by viruses directly but through infected tumor cells. This modeling aspect is consistent with the works [16–18]. Additionally, [22] distinguishes adaptive immune cells into those that are either tumor-specific or virus-specific, where virus-specific adaptive immune cells do kill viruses. Therefore, even the adaptive immune cells are capable of killing viruses according to Murphy

et al. [21] and the studies by Vithanage et al., and Storey et al. [17, 18, 22]. The killings of sensitive, resistant, and infected tumor cells, as well as viruses, by immune cells are modeled using a simple mass action approach, with maximal rates denoted by k_s, k_r, k_i, and k_v, respectively.

The interaction between sensitive cancer cells and viruses obeys the simple law of mass action where β denotes the maximum rate. The parameter b denotes an extra mortality rate of infected cancer cells due to infection, which quantifies pathogenicity of the virus. When infected cancer cells die, new viral progeny are discharged. The number of viruses released per infected tumor cell is represented by q. The viral clearance rate is represented by the parameter c. Every parameter is positive except potentially for d and a. Here, $d \geq 0$ denotes the rate of transition from resistance to sensitivity. Parameters a and d are identified as the Darwinian effect in [5] when studying acquired resistance in chemotherapy. With respect to resistance in OVT, the transition from resistance to sensitivity could be influenced by the solid tumor's geometric characteristics. After the demise of certain infected cancer cells, specific resistant cancer cells may become susceptible to infection and consequently transition to a sensitive state. Moreover, the drug ruxolitinib is employed to deal with pancreatic ductal adenocarcinoma (PDAC) cells that are not sensitive to oncolytic vesicular stomatitis virus (VSV), improving the susceptibility of resistant pancreatic cancer cells to VSV [23]. This treatment may result in an increase in d because of resistance therapy.

The immune cells are recruited by tumor cells using a Michaelis-Menten function $\dfrac{\alpha(T_s + T_r + T_i)Z}{m + T_s + T_r + T_i}$, where α represents the maximal proliferation rate, and m is the half-saturation constant. Immune cells can be eliminated or depleted through various processes, such as cell death (apoptosis), clearance by other immune cells, or inhibition of immune cell production [3]. We assume that this eliminate rate is constant and is denoted by the parameter γ. To incorporate the time delay between the encounter with tumor cells and the proliferation of immune cells, we introduce a discrete delay parameter, denoted as τ, into the activation term.

From the above discussion, the interaction between various types of tumor cells, viruses, and immune cells can be captured by the following system:

$$\begin{aligned}
T_s'(t) &= r_s T_s(t)\Big(1 - \frac{T_s(t) + T_r(t)}{K}\Big) - aT_s(t) - \beta T_s(t)V(t) + dT_r(t) - k_s T_s(t)Z(t)\\
T_r'(t) &= r_r T_r(t)\Big(1 - \frac{T_s(t) + T_r(t)}{K}\Big) + aT_s(t) - dT_r(t) - k_r T_r(t)Z(t)\\
T_i'(t) &= \beta T_s(t)V(t) - bT_i(t) - k_i T_i(t)Z(t)\\
V'(t) &= qbT_i(t) - cV(t) - k_v V(t)Z(t)\\
Z'(t) &= \frac{\alpha\Big(T_s(t-\tau) + T_r(t-\tau) + T_i(t-\tau)\Big)Z(t-\tau)}{m + T_s(t-\tau) + T_r(t-\tau) + T_i(t-\tau)} - \gamma Z(t).
\end{aligned} \tag{2.1}$$

The initial data on $[-\tau, 0]$ are given by

$$\begin{aligned}
&T_s(t) = \phi_1(t),\ T_r(t) = \phi_2(t),\ T_i(t) = \phi_3(t),\ V(t) = \phi_4(t),\ Z(t) = \phi_5(t),\ t \in [-\tau, 0],\\
&\phi_j(t) \in C([-\tau, 0], \mathbb{R}_+),\ 1 \leq j \leq 5,\ \phi_1(0) > 0,\ \phi_1(0) + \phi_2(0) \leq K,
\end{aligned} \tag{2.2}$$

where $C([-\tau, 0], \mathbb{R}_+)$ represents the Banach space of all continuous functions mapping the interval $[-\tau, 0]$ into $\mathbb{R}_+ = \{x \in \mathbb{R} : x \geq 0\}$. A conceptual diagram of model (2.1) is given in Figure 1.

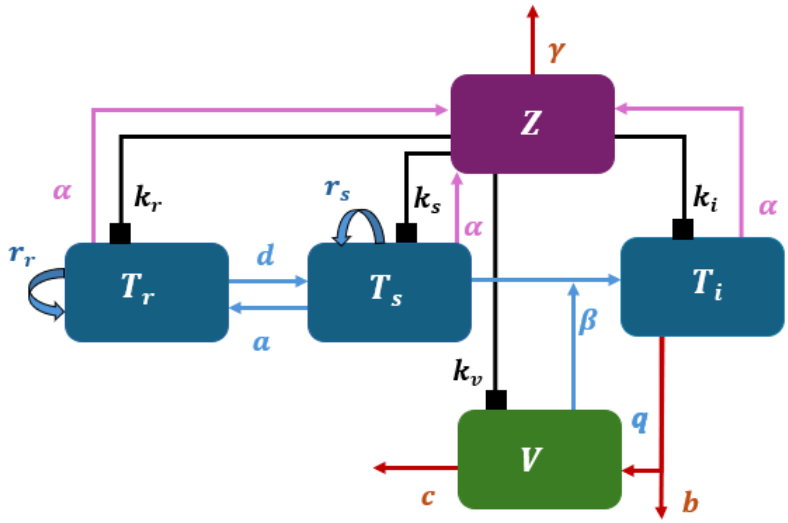

Figure 1. A schematic diagram of model (2.1), illustrating the interactions between different populations, is presented. Specifically, T_s, T_r, and T_i in blue boxes represent sensitive, resistant, and infected tumor cell compartments, respectively. The variable V in a green box denotes free viruses, and Z in a purple box represents the immune cell compartment. Parameters r_s and r_r are the growth rates of sensitive and resistant tumor cells, respectively. Parameter c is the viral clearance rate, and β denotes the virus transmission rate. The parameter q represents the virus burst size per infected tumor cell, while a is the rate of mutation of sensitive cancer cells. The parameter d is the rate of transition from resistance to sensitivity. Parameters k_s, k_r, k_i, and k_v denote the maximal killing rates of T_s, T_r, T_i, and V, respectively, due to immune cells. γ is the death rate of immune cells, and α represents the maximal immune cell proliferation rate. Traditional arrows denote the activation/transition/growth from one compartment to another, while block-head arrows denote killing or inhibition.

Let

$$\begin{aligned} X &= (x_1,\ x_2,\ x_3,\ x_4) = (T_s(t),\ T_r(t),\ T_i(t),\ V(t)) \\ Y &= (y_1,\ y_2,\ y_3,\ y_4) = (T_s(t-\tau),\ T_r(t-\tau),\ T_i(t-\tau),\ V(t-\tau)), \end{aligned} \tag{2.3}$$

and denote the right hand side of (2.1) as

$$f(X,Y) = (f_1(X,Y),\ f_2(X,Y),\ f_3(X,Y),\ f_4(X,Y)). \tag{2.4}$$

In the following, we verify that model (2.1) is well-posed and ensure that the model is biologically feasible. Its proof is relegated to Appendix C.

Theorem 2.1. *The solution to the systems* (2.1) *and* (2.2) *exists for* $t > 0$*, and is nonnegative and bounded.*

We next proceed to study model (2.1) without considering the delay in the activation of immune cells.

3. Analysis of ODE models

In this section, we shall investigate model (2.1) without delay, $\tau = 0$. Specifically, we study the ODE model without OVT in Section 3.1. The full system (2.1) with $\tau = 0$ is investigated in Section 3.2. The models of the special cases $d = 0$ and no resistant tumor cells are briefly discussed at the end of this section, and a more detailed discussion is presented in Appendix A.

3.1. The model with no viral therapy

Suppose $d > 0$. When $\tau = 0$ and there is no viral therapy, $T_i(0) = 0 = V(0)$, $T_i(t) = 0 = V(t)$ for $t > 0$, and (2.1) is reduced to

$$\begin{aligned}
T_s'(t) &= r_s T_s(t)\Big(1 - \frac{T_s(t) + T_r(t)}{K}\Big) - aT_s(t) + dT_r(t) - k_s T_s(t)Z(t)\\
T_r'(t) &= r_r T_r(t)\Big(1 - \frac{T_s(t) + T_r(t)}{K}\Big) + aT_s(t) - dT_r(t) - k_r T_r(t)Z(t)\\
Z'(t) &= \frac{\alpha(T_s(t) + T_r(t))Z(t)}{m + T_s(t) + T_r(t)} - \gamma Z(t)\\
T_s(0) &> 0,\ T_r(0) \geq 0,\ T_s(0) + T_r(0) \leq K,\ Z(0) \geq 0.
\end{aligned} \tag{3.1}$$

In addition, $Z(0) = 0$ implies $Z(t) = 0$ for $t > 0$, and (3.1) reduces to the two-dimensional T_sT_r system. The T_sT_r subsystem of (3.1) has been studied in [15]. The subsystem has two equilibria: $(0, 0)$ and $(\hat{T}_s, \hat{T}_r)$, with

$$\hat{T}_s = \frac{dK}{a + d}, \quad \hat{T}_r = \frac{aK}{a + d}, \tag{3.2}$$

where $(\hat{T}_s, \hat{T}_r)$ is globally asymptotically stable as shown in [15]. Consequently, (3.1) always has two equilibria $(0, 0, 0)$ and $(\hat{T}_s, \hat{T}_r, 0)$. The Jacobian matrix of (3.1) evaluated at $(0, 0, 0)$ and $(\hat{T}_s, \hat{T}_r, 0)$ is given respectively by

$$\begin{bmatrix} r_s - a & d & 0\\ a & r_r - d & 0\\ 0 & 0 & -\gamma \end{bmatrix}, \quad \text{and} \quad \begin{bmatrix} -r_s\hat{T}_s/K - a & -r_s\hat{T}_s/K + d & -k_s\bar{T}_s\\ -r_r\hat{T}_r/K + a & -r_r\hat{T}_r/K - d & -k_r\hat{T}_r\\ 0 & 0 & \dfrac{\alpha K}{m + K} - \gamma \end{bmatrix}. \tag{3.3}$$

It is evident that the stability of the equilibrium point $(0, 0, 0)$ hinges on the eigenvalues of the matrix

$$\begin{bmatrix} r_s - a & d\\ a & r_r - d \end{bmatrix}.$$

In the proof of Proposition 3.1 in [15], it is established that the eigenvalues of this matrix have positive real parts. Therefore, it follows that the equilibrium point $(0, 0, 0)$ is unstable. From (3.3), the stability of $(\hat{T}_s, \hat{T}_r, 0)$ is determined by the eigenvalues of the left upper 2×2 submatrix, which is Eq (3.3) of [15], and the sign of

$$\frac{\alpha K}{m + K} - \gamma.$$

It was shown in [15, Proposition 3,1] that the eigenvalues of the submatrix have negative real parts. As a result, $(\hat{T}_s, \hat{T}_r, 0)$ is asymptotically stable if $\dfrac{\alpha K}{m+K} < \gamma$ and unstable if $\dfrac{\alpha K}{m+K} > \gamma$. Let

$$\Gamma = \{(x, y, z) \in \mathbb{R}^3_+ : 0 < x + y \leq K\}. \tag{3.4}$$

Based on the proof provided in Appendix C, we can conclude that $(\hat{T}_s, \hat{T}_r, 0)$ is globally asymptotically stable in Γ if $\dfrac{\alpha K}{m+K} < \gamma$.

Proposition 3.1. *Let $\tau = 0$, $d > 0$, and $\dfrac{\alpha K}{m+K} < \gamma$. The equilibrium $(\hat{T}_s, \hat{T}_r, 0)$ is globally asymptotically stable in Γ for* (3.1).

The fraction $\dfrac{\alpha K}{m+K}$ is the maximal proliferation rate of immune cells induced by cancer cells. If this maximal rate is lower than the rate of immune cell death γ, the effector cells cannot sustain themselves, and the immune-free equilibrium $(\hat{T}_s, \hat{T}_r, 0)$ becomes globally asymptotically stable.

A positive equilibrium is an equilibrium in which each of its components is positive. To study the existence of positive equilibria, we assume $\dfrac{\alpha K}{m+K} > \gamma$ by Proposition 3.1, since if the inequality is reversed, solutions all converge to $(\hat{T}_s, \hat{T}_r, 0)$, and a positive equilibrium cannot exist. It follows that $\alpha > \gamma$. Define

$$\xi = \frac{m\gamma}{\alpha - \gamma}. \tag{3.5}$$

Setting $Z' = 0$ and $Z > 0$, we obtain $T_s + T_r = \xi$. Next, $T_s' = 0$ and $T_r' = 0$, imply respectively,

$$Z = \frac{r_s T_s(1 - \xi/K) - aT_s + d(\xi - T_s)}{k_s T_s} \quad \text{and} \quad Z = \frac{r_r(\xi - T_s)(1 - \xi/K) + aT_s - d(\xi - T_s)}{k_r(\xi - T_s)}.$$

Setting the above two expressions of Z equal, leads to the following second degree polynomial equation in T_s:

$$g(T_s) := \mathbf{a_1} T_s^2 + \mathbf{a_2} T_s + \mathbf{a_3} = 0, \tag{3.6}$$

where

$$\begin{aligned} \mathbf{a_1} &= \frac{[(a + d - r_s)k_r - k_s(a + d - r_r)]K + \xi(k_r r_s - k_s r_r)}{K}, \\ \mathbf{a_2} &= -\xi\frac{[(a + 2d - r_s)k_r - k_s(d - r_r)]K + \xi(k_r r_s - k_s r_r)}{K}, \\ \mathbf{a_3} &= \xi^2 d k_r. \end{aligned} \tag{3.7}$$

In addition, $g(\xi) = -k_s\xi^2 a < 0$, and $g(0) = \mathbf{a_3} > 0$. Since $T_r = \xi - T_s$ holds for the two components of any positive equilibrium, we therefore require the root $T_s < \xi$ as well. Also, setting $0 = T_s' + T_r'$, we have

$$Z = \frac{(r_s T_s + r_r T_r)(1 - \xi/K)}{k_s T_s + k_r T_r} > 0$$

provided $\xi < K$. i.e., $\xi < K$ is a necessary condition for the existence of a positive equilibrium. Notice $\xi < K$ is equivalent to $\dfrac{\alpha K}{m+K} > \gamma$, under which $(\hat{T}_s, \hat{T}_r, 0)$ is unstable.

We separate the discussion of $g(T_s) = 0$ into the cases of $\mathbf{a_1} < 0$, $\mathbf{a_1} > 0$, and $\mathbf{a_1} = 0$. If $\mathbf{a_1} < 0$, then it is evident that (3.1) exhibits an interior equilibrium uniquely since $g(\xi) < 0$. If $\mathbf{a_1} > 0$, then since $g(\xi) < 0$, $g(x) = 0$ has 2 positive roots x_1 and x_2 with $x_1 < \xi < x_2$. It follows that (3.1) also has a unique positive equilibrium. If $\mathbf{a_1} = 0$, then $\mathbf{a_2} = -\xi(ak_s + dk_r) < 0$, and thus there exists a unique positive equilibrium. We conclude that (3.1) exhibits a unique interior steady state $(\bar{T}_s, \bar{T}_r, \bar{Z})$ if $\dfrac{\alpha K}{m+K} > \gamma$.

Let $\dfrac{\alpha K}{m+K} > \gamma$ and let $J = (\bar{j}_{ij})$ denote the Jacobian matrix of (3.1) at $(\bar{T}_s, \bar{T}_r, \bar{Z})$, where

$$\begin{aligned}
&\bar{j}_{11} = -r_s\frac{\bar{T}_s}{K} - d\frac{\bar{T}_r}{\bar{T}_s}, \quad \bar{j}_{12} = d - r_s\frac{\bar{T}_s}{K}, \quad \bar{j}_{13} = -k_s\bar{T}_s,\\
&\bar{j}_{21} = a - r_r\frac{\bar{T}_r}{K}, \quad \bar{j}_{22} = -r_r\frac{\bar{T}_r}{K} - a\frac{\bar{T}_s}{\bar{T}_r}, \quad \bar{j}_{23} = -k_r\bar{T}_r,\\
&\bar{j}_{31} = \frac{\alpha m\bar{Z}}{(m+\bar{T}_s+\bar{T}_r)^2}, \quad \bar{j}_{32} = \bar{j}_{31}, \quad \bar{j}_{33} = 0.
\end{aligned} \tag{3.8}$$

Observe that

$$\bar{j}_{11}\bar{j}_{22} - \bar{j}_{21}\bar{j}_{12} = \frac{(\bar{T}_s+\bar{T}_r)\left(r_r d(\bar{T}_r)^2 + r_s a(\bar{T}_s)^2\right)}{K\bar{T}_s\bar{T}_r} > 0$$

and the characteristic polynomial is given by

$$\bar{P}_2(\lambda) = \lambda^3 + b_1\lambda^2 + b_2\lambda + b_3, \tag{3.9}$$

where

$$\begin{aligned}
&b_1 = -(\bar{j}_{11} + \bar{j}_{22}) > 0, \quad b_2 = (\bar{j}_{11}\bar{j}_{22} - \bar{j}_{12}\bar{j}_{21}) - (\bar{j}_{13} + \bar{j}_{23})\bar{j}_{31} > 0,\\
&b_3 = \bar{j}_{31}\left(\bar{j}_{11}\bar{j}_{23} + (\bar{j}_{22} - \bar{j}_{21})\bar{j}_{13} - \bar{j}_{12}\bar{j}_{23}\right).
\end{aligned} \tag{3.10}$$

Notice

$$\bar{j}_{11}\bar{j}_{23} + (\bar{j}_{22} - \bar{j}_{21})\bar{j}_{13} - \bar{j}_{12}\bar{j}_{23} = \frac{(\bar{T}_r+\bar{T}_s)((\bar{T}_r)^2 dk_r + (\bar{T}_s)^2 ak_s)}{\bar{T}_s+\bar{T}_r} > 0,$$

and thus $b_3 > 0$.

By the Routh-Hurwitz condition [24], $Re(\lambda) < 0$ for all roots of $\bar{P}_2(\lambda) = 0$ if and only if $b_1 > 0$, $b_3 > 0$, and $b_1 b_2 > b_3$. Since $b_1 > 0$ and $b_3 > 0$, $(\bar{T}_s, \bar{T}_r, \bar{Z})$ is locally asymptotically stable for system (3.1) if the condition

$$b_1 b_2 > b_3 \tag{3.11}$$

is satisfied. We cannot obtain a simplified expression of (3.11) involving components of the equilibrium, so we leave (3.11) as it is. The above discussion is summarized as follows.

Proposition 3.2. *Let $d > 0$ and $\dfrac{\alpha K}{m+K} > \gamma$. Then,* (3.1) *exhibits a unique interior steady state $(\bar{T}_s, \bar{T}_r, \bar{Z})$, which is asymptotically stable if* (3.11) *is valid, and unstable if* (3.11) *is reversed.*

The existence condition of a unique interior equilibrium implies that

$$\bar{T}_s + \bar{T}_r = \xi < K = \hat{T}_s + \hat{T}_r,$$

and therefore the total tumor load in $(\bar{T}_s, \bar{T}_r, \bar{Z})$ is smaller than the corresponding tumor burden in $(\hat{T}_s, \hat{T}_r, 0)$. The immune cells are able to reduce the total tumor load if their maximal proliferation rate is greater than their death rate.

3.2. The full model

We assume $d > 0$ and investigate the full system (2.1) without delay by examining the existence and stability of equilibria. The Jacobian matrix has the following entries:

$$\begin{aligned}
&j_{11} = r_s(1 - \frac{2T_s + T_r}{K}) - a - \beta V - k_s Z, \quad j_{12} = -r_s\frac{T_s}{K} + d, \quad j_{13} = 0,\\
&j_{14} = -\beta T_s, \quad j_{15} = -k_s T_s, \quad j_{21} = -r_r\frac{T_r}{K} + a, \quad j_{22} = r_r(1 - \frac{T_s + 2T_r}{K}) - d - k_r Z,\\
&j_{23} = 0, \quad j_{24} = 0, \quad j_{25} = -k_r T_r, \quad j_{31} = \beta V, \quad j_{32} = 0, \quad j_{33} = -b - k_i Z,\\
&j_{34} = \beta T_s, \; j_{35} = -k_i T_i, \quad j_{41} = 0, \; j_{42} = 0, \quad j_{43} = qb, \quad j_{44} = -c - k_v Z,\\
&j_{45} = -k_v V, \quad j_{51} = \frac{\alpha m Z}{(m + T_s + T_r)^2}, \quad j_{52} = j_{51}, \quad j_{53} = j_{51},\\
&j_{54} = 0, \quad j_{55} = \frac{\alpha(T_s + T_r + T_i)}{m + T_s + T_r + T_i} - \gamma.
\end{aligned} \tag{3.12}$$

Denote the two equilibria by $E_0 = (0, 0, 0, 0, 0)$ and $E_1 = (\hat{T}_s, \hat{T}_r, 0, 0, 0)$, where $\hat{T}_s + \hat{T}_r = K$. At E_0, the Jacobian matrix becomes

$$J(E_0) = \begin{bmatrix} r_s - a & d & 0 & 0 & 0\\ a & r_r - d & 0 & 0 & 0\\ 0 & 0 & -b & 0 & 0\\ 0 & 0 & qb & -c & 0\\ 0 & 0 & 0 & 0 & -\gamma \end{bmatrix}.$$

Eigenvalues of $J(E_0)$ are the eigenvalues of

$$\begin{bmatrix} r_s - a & d\\ a & r_r - d \end{bmatrix}, \quad -b, \quad -c, \quad \text{and} \quad -\gamma.$$

Therefore, E_0 is always unstable. At E_1,

$$J(E_1) = \begin{bmatrix} -r_s\frac{\hat{T}_s}{K} - a & -r_s\frac{\hat{T}_s}{K} + d & 0 & -\beta\hat{T}_s & -k_s\hat{T}_s\\ -r_r\frac{\hat{T}_r}{K} + a & -r_r\frac{\hat{T}_r}{K} - d & 0 & 0 & -k_r\hat{T}_r\\ 0 & 0 & -b & \beta\hat{T}_s & 0\\ 0 & 0 & qb & -c & 0\\ 0 & 0 & 0 & 0 & \frac{\alpha K}{m + K} - \gamma \end{bmatrix}.$$

The eigenvalues consist of the eigenvalues of the upper left 2×2 and the lower right 3×3 submatrices. It follows that E_1 is locally asymptotically stable if

$$c > \beta q \hat{T}_s \quad \text{and} \quad \frac{\alpha K}{m + K} < \gamma.$$

The stability of E_0 and E_1 is summarized below.

Proposition 3.3. *Let $\tau = 0$ and $d > 0$. System (2.1) always has two equilibria $E_0 = (0, 0, 0, 0, 0)$ and $E_1 = (\hat{T}_s, \hat{T}_r, 0, 0, 0)$, where E_0 is unstable. The equilibrium E_1 is asymptotically stable if $c > \beta q \hat{T}_s$ and $\frac{\alpha K}{m + K} < \gamma$, and unstable if either $c < \beta q \hat{T}_s$ or $\frac{\alpha K}{m + K} > \gamma$.*

In the following, we show that there will be no viruses and infected tumor cells if the viral death rate c is sufficiently large. Since the proof is similar to that given in [17], it is omitted.

Proposition 3.4. *If $c > \beta q K$, then solutions of (2.1) with $\tau = 0$ satisfy $\lim_{t \to \infty} T_i(t) = 0 = \lim_{t \to \infty} V(t)$.*

Based on Proposition 3.4, we provide a global asymptotic stability result of E_1 under some constraints. Its proof is presented in Appendix C. Let

$$D = \{(X, Y, Z, V, W) \in \mathbb{R}^5_+ : 0 < X + Y \leq K\}. \tag{3.13}$$

Theorem 3.1. *Let $\tau = 0$ and $d > 0$. If $c > \beta q K$ and $\frac{\alpha K}{m + K} < \gamma$, then $E_1 = (\hat{T}_s, \hat{T}_r, 0, 0, 0)$ is globally asymptotically stable in D.*

The lump parameter $\beta q K$ can be viewed as the maximal virus production rate. If this rate is smaller than the viral clearance rate c, and the maximal proliferation rate of immune cells is not large enough, $\frac{\alpha K}{m + K} < \gamma$, then neither the effector cells nor the viruses can persist in the system.

Suppose now the maximal proliferation rate of effector cells exceeds their death rate, $\frac{\alpha K}{m + K} > \gamma$. Then (2.1) has an equilibrium of the form $E_2 = (\bar{T}_s, \bar{T}_r, 0, 0, \bar{Z})$, where $(\bar{T}_s, \bar{T}_r, \bar{Z})$ is the positive equilibrium of the virus-free subsystem (3.1). Its stability depends on the eigenvalues of

$$J(E_2) = \begin{bmatrix} \bar{j}_{11} & \bar{j}_{12} & 0 & j_{14} & \bar{j}_{13} \\ \bar{j}_{21} & \bar{j}_{22} & 0 & 0 & \bar{j}_{23} \\ 0 & 0 & j_{33} & j_{34} & 0 \\ 0 & 0 & j_{43} & j_{44} & 0 \\ \bar{j}_{31} & \bar{j}_{31} & \bar{j}_{31} & 0 & 0 \end{bmatrix}, \tag{3.14}$$

where $\bar{J}_{ik}$, $1 \leq i, k \leq 2$, and $\bar{j}_{13}, \bar{j}_{23}, \bar{j}_{31}$ are defined in (3.8). By interchanging columns 3 and 5, and the corresponding rows, $J(E_2)$ is similar to

$$\begin{bmatrix} \bar{j}_{11} & \bar{j}_{12} & \bar{j}_{13} & j_{14} & 0 \\ \bar{j}_{21} & \bar{j}_{22} & \bar{j}_{23} & 0 & 0 \\ \bar{j}_{31} & \bar{j}_{31} & 0 & 0 & \bar{j}_{31} \\ 0 & 0 & 0 & j_{44} & j_{43} \\ 0 & 0 & 0 & j_{34} & j_{33} \end{bmatrix}. \tag{3.15}$$

It follows that the characteristic polynomial of $J(E_2)$ is the product of $\bar{P}_2(\lambda)$ defined in (3.9) and

$$\lambda^2 - (j_{33} + j_{44})\lambda + j_{33}j_{44} - j_{34}j_{43}.$$

Since $j_{33} < 0$, $j_{44} < 0$, $j_{34} > 0$ and $j_{43} > 0$, in addition to the condition of (3.11), one would also require $j_{33}j_{44} - j_{34}j_{43} > 0$, i.e.,

$$(b + k_i\bar{Z})(c + k_v\bar{Z}) - \beta qb\bar{T}_s > 0 \tag{3.16}$$

for E_2 to be locally asymptotically stable.

Proposition 3.5. *Let $\tau = 0$ and $\dfrac{\alpha K}{m + K} > \gamma$. Then,* (2.1) *has the equilibrium $E_2 = (\bar{T}_s, \bar{T}_r, 0, 0, \bar{Z})$, where E_2 is asymptotically stable if* (3.11) *and* (3.16) *are satisfied, and E_2 is unstable if the inequality in* (3.11) *or* (3.16) *is reversed.*

Observe that system (2.1) has an equilibrium of the form $E_3 = (T_s^*, T_r^*, T_i^*, V^*, 0)$, provided $c < \beta q\hat{T}_s$, where $(T_s^*, T_r^*, T_i^*, V^*)$ is the unique positive equilibrium in the tumor-virus subsystem without immune cells by a previous analysis [15]. In particular,

$$T_s^* = \frac{c}{\beta q}, \quad T_r^* = \frac{K(r_r - d - r_r T_s^*/K) + K\sqrt{(r_r - d - r_r T_s^*/K)^2 + 4aT_s^* r_r/K}}{2r_r},$$

$$V^* = \frac{(r_s T_s^* + r_r T_r^*)(1 - \dfrac{T_s^* + T_r^*}{K})}{\beta T_s^*}, \quad T_i^* = \frac{\beta T_s^* V^*}{b}.$$

The equilibrium E_3 has the Jacobian matrix given by

$$J(E_3) = \begin{pmatrix} a_{11} & a_{12} & 0 & a_{14} & a_{15} \\ a_{21} & a_{22} & 0 & 0 & a_{25} \\ a_{31} & 0 & a_{33} & a_{34} & a_{35} \\ 0 & 0 & a_{43} & a_{44} & a_{45} \\ 0 & 0 & 0 & 0 & a_{55} \end{pmatrix}, \tag{3.17}$$

where

$$\begin{aligned} &a_{11} = -(\frac{dT_r^*}{T_s^*} + \frac{r_s T_s^*}{K}), \quad a_{12} = d - \frac{r_s T_s^*}{K}, \quad a_{14} = -\beta T_s^*, \quad a_{15} = -k_s T_s^*, \\ &a_{21} = a - \frac{r_r T_r^*}{K}, \quad a_{22} = -(\frac{aT_s^*}{T_r^*} + \frac{r_r T_r^*}{K}), \quad a_{25} = -k_r T_r^*, \quad a_{31} = \beta V^*, \\ &a_{33} = -b, \quad a_{34} = \beta T_s^*, \quad a_{35} = -k_i T_i^*, \quad a_{43} = qb, \\ &a_{44} = -c, \quad a_{45} = -k_v V^*, \quad a_{55} = \frac{\alpha(T_s^* + T_r^* + T_i^*)}{m + T_s^* + T_r^* + T_i^*} - \gamma. \end{aligned} \tag{3.18}$$

The characteristic polynomial of $J(E_3)$ can be expressed by

$$P_3(\lambda) = (\lambda - a_{55})(\lambda^4 + a_1\lambda^3 + a_2\lambda^2 + a_3\lambda + a_4),$$

where $a_i,\ 1 \le i \le 4$, are given as

$$\begin{aligned} a_4 &= \Big((a_{33}a_{44} - a_{34}a_{43})a_{11} + a_{31}a_{14}a_{43}\Big)a_{22} - a_{12}a_{21}(a_{33}a_{44} - a_{34}a_{43}) > 0, \\ a_3 &= \Big(-(a_{33} + a_{44})a_{11} - a_{33}a_{44} + a_{34}a_{43}\Big)a_{22} + (-a_{33}a_{44} + a_{34}a_{43})a_{11} \\ &+ a_{12}a_{21}a_{44} + a_{12}a_{21}a_{33} - a_{14}a_{43}a_{31} > 0, \\ a_2 &= (a_{11} + a_{33} + a_{44})a_{22} + a_{33}a_{44} - a_{12}a_{21} - a_{34}a_{43} + (a_{33} + a_{44})a_{11} > 0, \\ a_1 &= -(a_{11} + a_{22} + a_{33} + a_{44}) > 0. \end{aligned} \tag{3.19}$$

By the Routh-Hurwitz criterion [24], E_3 is asymptotically stable if

$$a_{55} < 0 \quad \textit{and} \quad a_1a_2a_3 > a_3^2 + a_4a_1^2. \tag{3.20}$$

We now summarize the stability properties of equilibrium point E_3.

Proposition 3.6. *Let $\tau = 0$ and $\beta q\hat{T}_s > c$. Then,* (2.1) *has an equilibrium of the form $E_3 = (T_s^*, T_r^*, T_i^*, V^*, 0)$, where E_3 is asymptotically stable if the inequalities in* (3.20) *are satisfied, and E_3 is unstable if $a_{55} > 0$ or $a_1a_2a_3 < a_3^2 + a_4a_1^2$.*

The conditions for the existence and local stability of the boundary equilibria of (2.1) with $\tau = 0$ are summarized in Table 1.

Table 1. The existence and stability conditions of boundary equilibria of system (2.1) with $\tau = 0$. The stability column provides sufficient conditions for the asymptotic stability of the corresponding equilibrium.

Boundary equilibrium (T_s, T_r, T_i, V, Z)	Existence	Stability
$E_0 = (0, 0, 0, 0, 0)$	Always	Unstable
$E_1 = (\hat{T}_s, \hat{T}_r, 0, 0, 0)$	Always	$c > \beta q\hat{T}_s$ and $\dfrac{\alpha K}{m+K} < \gamma$
$E_2 = (\bar{T}_s, \bar{T}_r, 0, 0, \bar{Z})$	$\dfrac{\alpha K}{m+K} > \gamma$	(3.11) and (3.16)
$E_3 = (T_s^*, T_r^*, T_i^*, V^*, 0)$	$c < \beta q\hat{T}_s$	(3.20)

In the cases where resistant tumor cells cannot be converted to sensitivity, for example, if there are no drugs available to reverse the resistance with OVT for a certain tumor type, then the parameter d is set to 0. We can provide a similar analysis as in the previous discussion and obtain some biological conclusions. In particular, according to Theorem A.1, every sensitive tumor cell becomes resistant, and there are no immune cells involved in the interaction if the following two conditions are met: First, the death rate c of viruses must exceed its maximum production rate βqK. Second, the immune cell activation rate $\dfrac{\alpha K}{m+K}$ must be smaller than its clearance rate γ. This result differs from the findings presented in [15], where it was shown that every tumor cell becomes resistant if $c > \beta qK$, as there were no immune cells to control the tumor.

For the situation of no resistant tumor cells, it represents the best-case scenario where the tumor cells are not resistant to OVT. From the analysis given in Appendix A.2, we conclude that even in the absence of resistance to OVT, therapy can fail if the virus death rate is high and the immune activation rate is low, as demonstrated in Theorem A.2.

4. Analysis of DDE models

The main goal of this section is to study the effects of delay τ on the stability of equilibria of model (2.1). Our discussion parallels the ODE model discussed in Section 3. Specifically, the model of no OVT is studied in Section 4.1, and Section 4.2 investigates the full system (2.1). The models with $d = 0$ and with no resistant tumor cells are briefly summarized at the end of Section 4.2, with a more detailed presentation given in Appendix B. For an analysis of the local stability of equilibria in DDE models, we refer the reader to the works of Hale [25], Kuang [26], and Smith [27].

4.1. The model of no OVT

Let $d > 0$. The three-dimensional model of delay differential equations without infected cancer cells is given as

$$\begin{aligned}
T_s'(t) &= r_s T_s(t)\Big(1 - \frac{T_s(t) + T_r(t)}{K}\Big) - aT_s(t) + dT_r(t) - k_s T_s(t)Z(t),\\
T_r'(t) &= r_r T_r(t)\Big(1 - \frac{T_s(t) + T_r(t)}{K}\Big) + aT_s(t) - dT_r(t) - k_r T_r(t)Z(t),\\
Z'(t) &= \frac{\alpha(T_s(t-\tau) + T_r(t-\tau))}{m + T_s(t-\tau) + T_r(t-\tau)}Z(t-\tau) - \gamma Z(t),\\
T_s(t) &= \psi_1(t),\ T_r(t) = \psi_2(t),\ Z(t) = \psi_3(t),\ t \in [-\tau, 0],\\
\psi_j(t) &\in C([-\tau, 0], \mathbb{R}_+),\ 1 \le j \le 3,\ \psi_1(0) > 0,\ \psi_1(0) + \psi_2(0) \le K.
\end{aligned} \tag{4.1}$$

The stability of an equilibrium $(\hat{X}_0, \hat{X}_0)$ of (4.1) depends on the stability of the linearized system

$$\mathbf{X}'(\mathbf{t}) = \hat{A}\mathbf{X}(\mathbf{t}) + \hat{B}\mathbf{X}(\mathbf{t} - \tau)$$

at the zero equilibrium. Here,

$$\hat{A} = \hat{f}_{\hat{X}}(\hat{X}_0, \hat{X}_0), \quad \text{and} \quad \hat{B} = \hat{f}_{\hat{Y}}(\hat{X}_0, \hat{X}_0),$$

where $\hat{f}$ refers to the right-hand side of (4.1) with $\hat{X}$ and $\hat{Y}$ similarly defined as in (2.3). The characteristic equation for the linearized system is given as

$$det(\lambda I - \hat{A} - \hat{B}e^{-\lambda\tau}) = 0.$$

At $\hat{X}_0 = (0, 0, 0)$, since

$$\hat{A} + \hat{B}e^{-\lambda\tau} = \begin{bmatrix} r_s - a & d & 0\\ a & r_r - d & 0\\ 0 & 0 & -\gamma \end{bmatrix}$$

does not depend on τ, $(0,0,0)$ remains unstable for $\tau > 0$. At $\hat{X}_0 = (\hat{T}_s, \hat{T}_r, 0)$,

$$\hat{A} + \hat{B}e^{-\lambda\tau} = \begin{bmatrix} -r_s\hat{T}_s/K - a & -r_s\hat{T}_s/K + d & -k_s\hat{T}_s \\ -r_r\hat{T}_r/K + a & -r_r\hat{T}_r/K - d & -k_r\hat{T}_r \\ 0 & 0 & \dfrac{\alpha K}{m+K}e^{-\lambda\tau} - \gamma \end{bmatrix},$$

where the upper left 2×2 submatrix is the Jacobian matrix of the two-dimensional T_sT_r ODE system evaluated at $(\hat{T}_s, \hat{T}_r)$, which was analyzed in [15, Proposition 3.1] with eigenvalues consisting of negative real parts. Therefore, the stability of $(\hat{T}_s, \hat{T}_r, 0)$ depends on the zeros of

$$\frac{\alpha K}{m+K}e^{-\lambda\tau} - \gamma.$$

Assume $\dfrac{\alpha K}{m+K} < \gamma$, i.e., $(\hat{T}_s, \hat{T}_r, 0)$ is stable asymptotically for the corresponding non-delay system. Consider

$$\frac{\alpha K}{m+K}e^{-\lambda\tau} - \gamma - \lambda = 0. \tag{4.2}$$

It is known that $\lambda = \dfrac{\alpha K}{m+K} - \gamma < 0$ when $\tau = 0$. If $(\hat{T}_s, \hat{T}_r, 0)$ alters its stability for some $\tau > 0$, then (4.2) will possess a pair of purely imaginary roots $\pm i\omega$, $\omega > 0$, at some $\tau > 0$. Replacing λ by iw in (4.2), we obtain the following two equations:

$$\frac{\alpha K}{m+K}\cos(\omega\tau) - \gamma = 0 \quad \text{and} \quad \frac{\alpha K}{m+K}\sin(\omega\tau) + \omega = 0.$$

Then, from the trigonometric identity $\cos^2(\theta) + \sin^2(\theta) = 1$ for $\theta \in \mathbb{R}$, it follows that $\omega > 0$ must satisfy

$$(m+K)^2\omega^2 + \gamma^2(m+K)^2 - \alpha^2k^2 = 0.$$

The quadratic equation has a unique root

$$\omega^2 = \frac{(\alpha K - \gamma(m+K))(\alpha K + \gamma(m+K))}{(m+K)^2} < 0$$

by the assumption. We obtain a contradiction and conclude that all the roots λ of (4.2) satisfy $Re(\lambda) < 0$. Therefore, $(\hat{T}_s, \hat{T}_r, 0)$ is asymptotically stable for all $\tau \geq 0$ if $\dfrac{\alpha K}{m+K} < \gamma$. The proof of the last part of Proposition 4.1(b) is presented in Appendix C.

Proposition 4.1. *The following statements hold for system* (4.1).

(a) $(0,0,0)$ *is always unstable for* $\tau \geq 0$.

(b) $(\hat{T}_s, \hat{T}_r, 0)$ *is asymptotically stable for all* $\tau \geq 0$ *if* $\dfrac{\alpha K}{m+K} < \gamma$, *and it is is unstable for all* $\tau \geq 0$ *if* $\dfrac{\alpha K}{m+K} > \gamma$.

Let $\dfrac{\alpha K}{m+K} > \gamma$ and the condition in (3.11) be satisfied. That is, (3.1) has the unique positive equilibrium $(\bar{T}_s, \bar{T}_r, \bar{Z})$ by Proposition 3.2 and is moreover asymptotically stable for the ODE model (3.1). Since

$$\frac{\alpha(\bar{T}_s + \bar{T}_r)}{m + \bar{T}_s + \bar{T}_r} = \gamma,$$

the stability of $(\bar{T}_s, \bar{T}_r, \bar{Z})$ depends on the eigenvalues of

$$\begin{bmatrix} \bar{j}_{11} & \bar{j}_{12} & \bar{j}_{13} \\ \bar{j}_{21} & \bar{j}_{22} & \bar{j}_{23} \\ \bar{j}_{31}e^{-\lambda\tau} & \bar{j}_{31}e^{-\lambda\tau} & -\gamma + \gamma e^{-\lambda\tau} \end{bmatrix}, \tag{4.3}$$

where $\bar{j}_{ik}$, $1 \le i,k \le 2$, $\bar{j}_{13}$, $\bar{j}_{23}$, and $\bar{j}_{31}$, defined in (3.8), are the entries of the Jacobian matrix of the ODE model (3.1) evaluated at $(\bar{T}_s, \bar{T}_r, \bar{Z})$. The determinantal equation for (4.3) can be written as

$$\lambda^3 + p_1\lambda^2 + p_2\lambda + p_3 + (-\gamma\lambda^2 + q_1\lambda + q_2)e^{-\lambda\tau} = 0, \tag{4.4}$$

where

$$\begin{aligned} &p_1 = \gamma - \bar{j}_{11} - \bar{j}_{22} > 0, \quad p_2 = (\bar{j}_{11}\bar{j}_{22} - \bar{j}_{12}\bar{j}_{21}) - \gamma(\bar{j}_{11} + \bar{j}_{22}) > 0, \\ &p_3 = (\bar{j}_{11}\bar{j}_{22} - \bar{j}_{12}\bar{j}_{21})\gamma > 0, \quad q_1 = (\bar{j}_{11} + \bar{j}_{22})\gamma - \bar{j}_{31}(\bar{j}_{13} + \bar{j}_{23}), \\ &q_2 = (-\bar{j}_{11}\bar{j}_{22} + \bar{j}_{12}\bar{j}_{21})\gamma + \bar{j}_{31}(\bar{j}_{11}\bar{j}_{23} - \bar{j}_{12}\bar{j}_{23} - \bar{j}_{13}\bar{j}_{21} + \bar{j}_{13}\bar{j}_{22}). \end{aligned} \tag{4.5}$$

If $(\bar{T}_s, \bar{T}_r, \bar{Z})$ undergoes a stability change for some $\tau > 0$, then (4.4) will have a pair of purely imaginary eigenvalues $\lambda = \pm i\omega$, $\omega > 0$, at some $\tau > 0$. Replacing λ by $i\omega$ in (4.4), we arrive at

$$p_1\omega^2 - p_3 = (\gamma\omega^2 + q_2)\cos(\omega\tau) + q_1\omega\sin(\omega\tau), \tag{4.6}$$

$$\omega^3 - p_2\omega = q_1\omega\cos(\omega\tau) - (\gamma\omega^2 + q_2)\sin(\omega\tau). \tag{4.7}$$

By squaring both sides of (4.6) and (4.7), and adding the resulting two equations, we have

$$\omega^6 + (p_1^2 - 2p_2 - \gamma^2)\omega^4 + (p_2^2 - 2p_1p_3 - 2\gamma q_2 - q_1^2)\omega^2 + p_3^2 - q_2^2 = 0. \tag{4.8}$$

In terms of $x = \omega^2$, Eq (4.8) becomes a polynomial equation of degree three:

$$F(x) := x^3 + (p_1^2 - 2p_2 - \gamma^2)x^2 + (p_2^2 - 2p_1p_3 - 2\gamma q_2 - q_1^2)x + p_3^2 - q_2^2 = 0. \tag{4.9}$$

Further, Eqs (4.6) and (4.7) imply

$$\sin(\omega\tau) = \frac{p_1q_1\omega^3 - p_3q_1\omega + (\gamma\omega^2 + q_2)(p_2\omega - \omega^3)}{(\gamma\omega^2 + q_2)^2 + q_1^2\omega^2} := \rho_s, \tag{4.10}$$

$$\cos(\omega\tau) = \frac{q_1\omega(\omega^3 - p_2\omega) + (p_1\omega^2 - p_3)(\gamma\omega^2 + q_2)}{(\gamma\omega^2 + q_2)^2 + q_1^2\omega^2} := \rho_c. \tag{4.11}$$

If (4.9) has no positive roots, then (4.4) has no pure imaginary roots, and $(\bar{T}_s, \bar{T}_r, \bar{Z})$ remains stable for all $\tau > 0$. Applying the Routh-Hurwitz criterion [24], all roots of (4.9) have negative real parts if and only if the following conditions are satisfied:

$$\begin{aligned} &p_1^2 - 2p_2 - \gamma^2 > 0, \quad p_3^2 - q_2^2 > 0, \\ &(p_1^2 - 2p_2 - \gamma^2)(p_2^2 - 2p_1p_3 - 2\gamma q_2 - q_1^2) > p_3^2 - q_2^2. \end{aligned} \tag{4.12}$$

We conclude the following with respect to the stability of $(\bar{T}_s, \bar{T}_r, \bar{Z})$.

Proposition 4.2. *Let* $\dfrac{\alpha K}{m+K} > \gamma$ *and suppose* (3.11) *holds true. Then,* $(\bar{T}_s, \bar{T}_r, \bar{Z})$ *is asymptotically stable for* $\tau > 0$ *if the inequalities in* (4.12) *are satisfied.*

On the other hand, if $F(x) = 0$ has a simple positive root, the following result is valid. The proof is presented in Appendix C.

Theorem 4.1. *Let* $\dfrac{\alpha K}{m+K} > \gamma$ *and assume* $(\bar{T}_s, \bar{T}_r, \bar{Z})$ *is asymptotically stable for* (3.1). *If* (4.9) *has at least one positive simple root, then one can find* $\tau_0 > 0$ *for which* $(\bar{T}_s, \bar{T}_r, \bar{Z})$ *is asymptotically stable for* $\tau \in [0, \tau_0)$ *and* $\mathrm{Sign}(\dfrac{dRe(\lambda)}{d\tau}|_{\tau=\tau_0}) \neq 0$.

It is expected that a Hopf bifurcation occurs at $\tau = \tau_0$, causing the equilibrium $(\bar{T}_s, \bar{T}_r, \bar{Z})$ to become unstable.

4.2. The full model

We assume $d > 0$. To study the effect of delay τ on the equilibria for the full model (2.1), we examine the eigenvalues of the Jacobian matrix $A + Be^{-\lambda\tau}$, where $A = f_X(X_0, X_0)$, $B = f_Y(X_0, X_0)$, and (X_0, X_0) is an arbitrary equilibrium. At $E_0 = (0, 0, 0, 0, 0)$,

$$A + Be^{-\lambda\tau} = \begin{bmatrix} r_s - a & d & 0 & 0 & 0 \\ a & r_r - d & 0 & 0 & 0 \\ 0 & 0 & -b & 0 & 0 \\ 0 & 0 & qb & -c & 0 \\ 0 & 0 & 0 & 0 & -\gamma \end{bmatrix}$$

does not depend on τ, and therefore E_0 is always unstable for $\tau \geq 0$. At $E_1 = (\hat{T}_s, \hat{T}_r, 0, 0, 0)$,

$$A + Be^{-\lambda\tau} = \begin{bmatrix} -r_s\hat{T}_s/K - a & -r_s\hat{T}_s/K + d & 0 & -\beta\hat{T}_s & -k_s\hat{T}_s \\ -r_r\hat{T}_r/K + a & -r_r\hat{T}_r/K - d & 0 & 0 & -k_r\hat{T}_r \\ 0 & 0 & -b & \beta\hat{T}_s & 0 \\ 0 & 0 & qb & -c & 0 \\ 0 & 0 & 0 & 0 & \dfrac{\alpha K}{m+K}e^{-\lambda\tau} - \gamma \end{bmatrix}$$

has eigenvalues consisting of the eigenvalues of the upper left 2×2 and the lower right 3×3 submatrices. We assume $\beta q\hat{T}_s < c$ and $\dfrac{\alpha K}{m+K} < \gamma$ to ensure that E_1 is asymptotically stable for the ODE system

(2.1) with $\tau = 0$. It follows that the stability of E_1 for the DDE model (2.1) then depends on Eq (4.2). By Proposition 4.1, we conclude that if $\beta q\hat{T}_s < c$ and $\dfrac{\alpha K}{m+K} < \gamma$, all of the eigenvalues of $A + Be^{-\lambda\tau}$ have negative real parts, and $E_1 = (\hat{T}_s, \hat{T}_r, 0, 0, 0)$ is asymptotically stable for all $\tau \geq 0$. If $\beta q\hat{T}_s > c$, then E_1 is clearly unstable. If $\dfrac{\alpha K}{m+K} > \gamma$, one can also show that E_1 is unstable by the proof of Proposition 3.5(b). The above discussion is summarized as follows.

Proposition 4.3. *The following statements are valid for system* (2.1).

(a) $E_0 = (0, 0, 0, 0, 0)$ *is always unstable for* $\tau \geq 0$.

(b) $E_1 = (\hat{T}_s, \hat{T}_r, 0, 0, 0)$ *is asymptotically stable for* $\tau \geq 0$ *if* $\beta q\hat{T}_s < c$ *and* $\dfrac{\alpha K}{m+K} < \gamma$, *whereas* E_1 *is unstable for all* $\tau \geq 0$ *if* $\beta q\hat{T}_s > c$ *or* $\dfrac{\alpha K}{m+K} > \gamma$.

Observe that Proposition 4.3 implies the delay in the immune activation has no effect on the tumor-free equilibrium E_0 as well as the immune-free equilibrium E_1.

Let $\dfrac{\alpha K}{m+K} > \gamma$. Then, $E_2 = (\bar{T}_s, \bar{T}_r, 0, 0, \bar{Z})$ exists, and its stability depends on the eigenvalues of

$$\begin{pmatrix} \bar{j}_{11} & \bar{j}_{12} & 0 & j_{14} & \bar{j}_{13} \\ \bar{j}_{21} & \bar{j}_{22} & 0 & 0 & \bar{j}_{23} \\ 0 & 0 & j_{33} & j_{34} & 0 \\ 0 & 0 & j_{43} & j_{44} & 0 \\ \bar{j}_{31}e^{-\lambda\tau} & \bar{j}_{31}e^{-\lambda\tau} & \bar{j}_{31}e^{-\lambda\tau} & 0 & -\gamma + \gamma e^{-\lambda\tau} \end{pmatrix} \tag{4.13}$$

with $\bar{j}_{ij}$ given in (3.8). The characteristic equation can be written as

$$\left(\lambda^2 - (j_{33} + j_{44})\lambda + j_{33}j_{44} - j_{34}j_{43}\right)\left(\lambda^3 + p_1\lambda^2 + p_2\lambda + p_3 + (-\gamma\lambda^2 + q_1\lambda + q_2)e^{-\lambda\tau}\right) = 0,$$

where p_i, $1 \leq i \leq 3$, and q_i, $1 \leq i \leq 2$, are defined in (4.5).

Assume E_2 is asymptotically stable for the ODE model, i.e., both conditions (3.11) and (3.16) hold. Then the two roots of

$$\lambda^2 - (j_{33} + j_{44})\lambda + j_{33}j_{44} - j_{34}j_{43} = 0$$

have negative real parts. The stability of E_2 therefore depends on the roots of (4.4), and we have the following conclusions.

Theorem 4.2. *Let* $d > 0$ *and let* $\dfrac{\alpha K}{m+K} > \gamma$. *Then,* $E_2 = (\bar{T}_s, \bar{T}_r, 0, 0, \bar{Z})$ *exists. Suppose (3.11) and (3.16) are satisfied. In addition, if* (4.12) *is true, then* E_2 *is asymptotically stable for* $\tau \geq 0$.

The delay may not affect the stability of the virus-free equilibrium E_2 in the presence of immune cells, provided that the parameters satisfy the conditions outlined in Theorem 4.2. On the other hand, if $F(x) = 0$ has positive root, then the following is true.

Theorem 4.3. *Let* $d > 0$ *and let* $\dfrac{\alpha K}{m+K} > \gamma$, *and* (3.11) *and* (3.16) *be satisfied. Assume* $F(x) = 0$ *exhibits at least one simple positive root. Then, one can find* $\tau_0 > 0$ *such that* $E_2 = (\bar{T}_s, \bar{T}_r, 0, 0, \bar{Z})$ *is asymptotically stable for* $\tau \in [0, \tau_0)$ *and* $\dfrac{dRe(\lambda)}{d\tau}|_{\tau=\tau_0} \neq 0$.

It follows that the delay τ in the immune cell proliferation can destabilize the equilibrium E_2. As τ increases beyond the critical value τ_0, the virus-free equilibrium E_2 becomes unstable, leading to oscillations in the tumor-virus-immune interaction as a result of the delay in immune recruitment.

Let $c < \beta q \hat{T}_s$. Then, $E_3 = (T_s^*, T_r^*, T_i^*, V^*, 0)$ exists, and the stability of E_3 depends on the corresponding Jacobian matrix, written as

$$\begin{pmatrix} a_{11} & a_{12} & 0 & a_{14} & a_{15} \\ a_{21} & a_{22} & 0 & 0 & a_{25} \\ a_{31} & 0 & a_{33} & a_{34} & a_{35} \\ 0 & 0 & a_{43} & a_{44} & a_{45} \\ 0 & 0 & 0 & 0 & -\gamma + (a_{55} + \gamma)e^{-\lambda\tau} \end{pmatrix}, \tag{4.14}$$

where a_{ij}, $1 \le i, j \le 5$, are defined in (3.18). The characteristic equation is given by

$$\left(\lambda + \gamma - (a_{55} + \gamma)e^{-\lambda\tau}\right)\left(\lambda^4 + a_1\lambda^3 + a_2\lambda^2 + a_3\lambda + a_4\right) = 0,$$

with a_i, $1 \le i \le 4$, defined in (3.18). Assume $a_{55} < 0$ and $a_1a_2a_3 > a_3^2 + a_1^2a_4$ such that E_3 is asymptotically stable for the ODE model. That is,

$$\lambda^4 + a_1\lambda^3 + a_2\lambda^2 + a_3\lambda + a_4 = 0$$

has only roots with negative real parts. Let

$$g(\lambda) = \lambda + \gamma - (a_{55} + \gamma)e^{-\lambda\tau},$$

where $\tau > 0$ is fixed. If $g(\lambda)$ has a pair of pure imaginary roots $\lambda = \pm iw$, $w > 0$, then $w^2 = a_{55}(a_{55} + 2\gamma)$, where $a_{55} < 0$ and $a_{55} + 2\gamma > 0$. We obtain a contradiction and conclude that all roots of $g(\lambda)$ have negative real parts. On the other hand, if $a_{55} > 0$, then $g(0) = -a_{55} < 0$, $g(\infty) = \infty$, and $g'(\lambda) > 0$ for $\lambda \ge 0$. Thus, $g(\lambda) = 0$ has one positive root. Therefore, E_3 is unstable. Further, E_3 is clearly unstable if $a_1a_2a_3 < a_3^2 + a_1^2a_4$. Below is a summary of the discussion.

Theorem 4.4. *Let $\beta q \hat{T}_s > c$. Then, the equilibrium $E_3 = (T_s^*, T_r^*, T_i^*, V^*, 0)$ exists, and the following statements hold true.*

(a) E_3 is asymptotically stable for $\tau \ge 0$ if $a_{55} < 0$ and $a_1a_2a_3 > a_3^2 + a_1^2a_4$.
(b) E_3 is unstable for $\tau \ge 0$ if either $a_{55} > 0$ or $a_1a_2a_3 < a_3^2 + a_1^2a_4$.

Comparing Theorem 4.4 with Proposition 3.6, we observe that the delay τ in immune cell proliferation does not affect the stability of the immune-free tumorous equilibrium E_3.

For the scenario of no conversion from resistance to sensitivity, it is concluded from Appendix B that the delay in the immune activation has no effects on the stability of the two equilibria $E_0 = (0, 0, 0, 0, 0)$ and $E_1^0 = (0, K, 0, 0, 0)$. In addition, if $\dfrac{\alpha K}{m + K} > \gamma$, then $E_2^0 = (0, \xi, 0, 0, \tilde{Z}^0)$ exists, where $\xi = \dfrac{m\gamma}{\alpha - \gamma}$ and $\tilde{Z}^0 = \dfrac{r_r}{k_r}(1 - \dfrac{\xi}{K})$. It follows from Appendix B.1 that the delay can destabilize E_2^0.

In the best scenario where there is no resistance to OVT, the four-dimensional T_sT_iVZ system is further reduced to the two-dimensional T_sZ system, as shown in (A.5), if no viruses and infected tumor cells are present. System (A.5) possesses an equilibrium of the form $(\xi, \tilde{Z})$, provided that $\frac{\alpha K}{m+K} > \gamma$, where ξ is defined in (3.5) and $\tilde{Z}$ is given in (A.6). Therefore, the four-dimensional system has an equilibriun of the form $(\xi, 0, 0, \tilde{Z})$. This equilibrium is no longer asymptotically stable for $\tau > 0$. The time delay τ can destabilize this equilibrium. However, it can be verified that the delay has no destabilization effects on the equilibria $E_0 = (0, 0, 0, 0)$ and $\tilde{E}_1 = (K, 0, 0, 0)$. In addition, when the parameters satisfy the conditions given in Theorem B.2(b), the tumorous equilibrium $\tilde{E}_2 = (\xi, 0, 0, \tilde{Z})$ in the presence of immune cells becomes unstable, as the delay τ passes beyond the critical value τ_0. Consequently, the tumor-virus-immune interaction may exhibit oscillations due to the time delay in the immune activation. For the equilibrium $\tilde{E}_3 = (\tilde{T}_s, \tilde{T}_i, \tilde{V}, 0)$, since there are no immune cells present in the equilibrium, it is trivial to verify that the delay cannot have any effect on its stability.

5. Numerical simulation

In this section, we employ numerical tools to study system (2.1), addressing the effects of immune cells compared to the previous work in [15] in Section 5.1, incorporating global sensitivity analysis as discussed in Section 5.2, and covering numerical techniques for bifurcation analysis in Section 5.3. Section 5.4 explores the impact of parameters such as the virus transmission rate and half-saturation constant of immune activation on treatment success. Additionally, Section 5.5 considers a combination therapy of OVT and CAR T-cell therapy.

5.1. Effects of immune cells

In our prior study [15], we explored the interactions between tumor cells and oncolytic viruses. This section now focuses on demonstrating the impact of immune cells, in comparison with our previous work. Initially, we compare the outcomes of models that do not incorporate delays in either viral infection or immune cell activation. For this comparison, we set the common parameter values in both the four-dimensional and five-dimensional systems to be identical to those in the parameter set given in [15, Eq (4.1)], as follows:

$$K = 1/(1.02 \times 10^{-9}), \quad r_s = 0.45, \quad r_r = 0.01 \times r_s, \quad b = 1.333,$$
$$q = 250, \quad c = 0.1, \quad d = 10^{-3}, \quad a = 1 \times 10^{-5}, \quad \beta = 7 \times 10^{-12}.$$

The initial conditions chosen are $(7 \times 10^6, 10^2, 0, 5 \times 10^6)$ for the model with no immune cells and $(7 \times 10^6, 10^2, 0, 5 \times 10^6, 2 \times 10^3)$ for the five-dimensional system. In numerous mouse experiments, such as those documented in [28, 29], researchers typically inoculate mice subcutaneously with either 10^6, 2×10^6, or 5×10^6 cancer cells. At the time of injection, it is generally assumed that no immune cells are present in the mice. To allow the immune cells to proliferate to a quantity of 2×10^3, we increase the tumor burden to 7×10^6 cells, while maintaining a small number of resistant tumor cells, around 100 in this case. The doses of oncolytic viruses (OVs) administered vary, ranging from 2×10^6 in [29] to 10^8 pfu in [28]. For this part of the numerical simulation, we select 5×10^6, but slight variations in the initial conditions should not impede our biological conclusions.

Figure 2(a) depicts the outcome of the four-dimensional $T_sT_rT_iV$ model before incorporating immune cells, while Figure 2(b)–(d) depicts the outcome of the ODE five-dimensional model (2.1) with $\tau = 0$ for various parameter values. Specifically, the additional parameters for the five-dimensional $T_sT_rT_iVZ$ model are set as follows: (b) $\gamma = 0.03,\ k_s = 1.9 \times 10^{-4},\ k_r = 1.9 \times 10^{-4},\ k_i = 4,\ k_v = 0.025,\ m = 500$ with varied $\alpha = 0.03,\ 0.035,\ 0.04$; (c) $\alpha = 0.035,\ k_s = 1.9 \times 10^{-4},\ k_r = 1.9 \times 10^{-4},\ k_i = 4,\ k_v = 0.025,\ m = 500$ with varied $\gamma = 0.03,\ 0.035,\ 0.04$; and (d) $\alpha = 0.035,\ \gamma = 0.03,\ k_s = 1.9 \times 10^{-4},\ k_r = 1.9 \times 10^{-4},\ k_i = 4,\ k_v = 0.025$ with varied $m = 500,\ 5000,\ 10^5$.

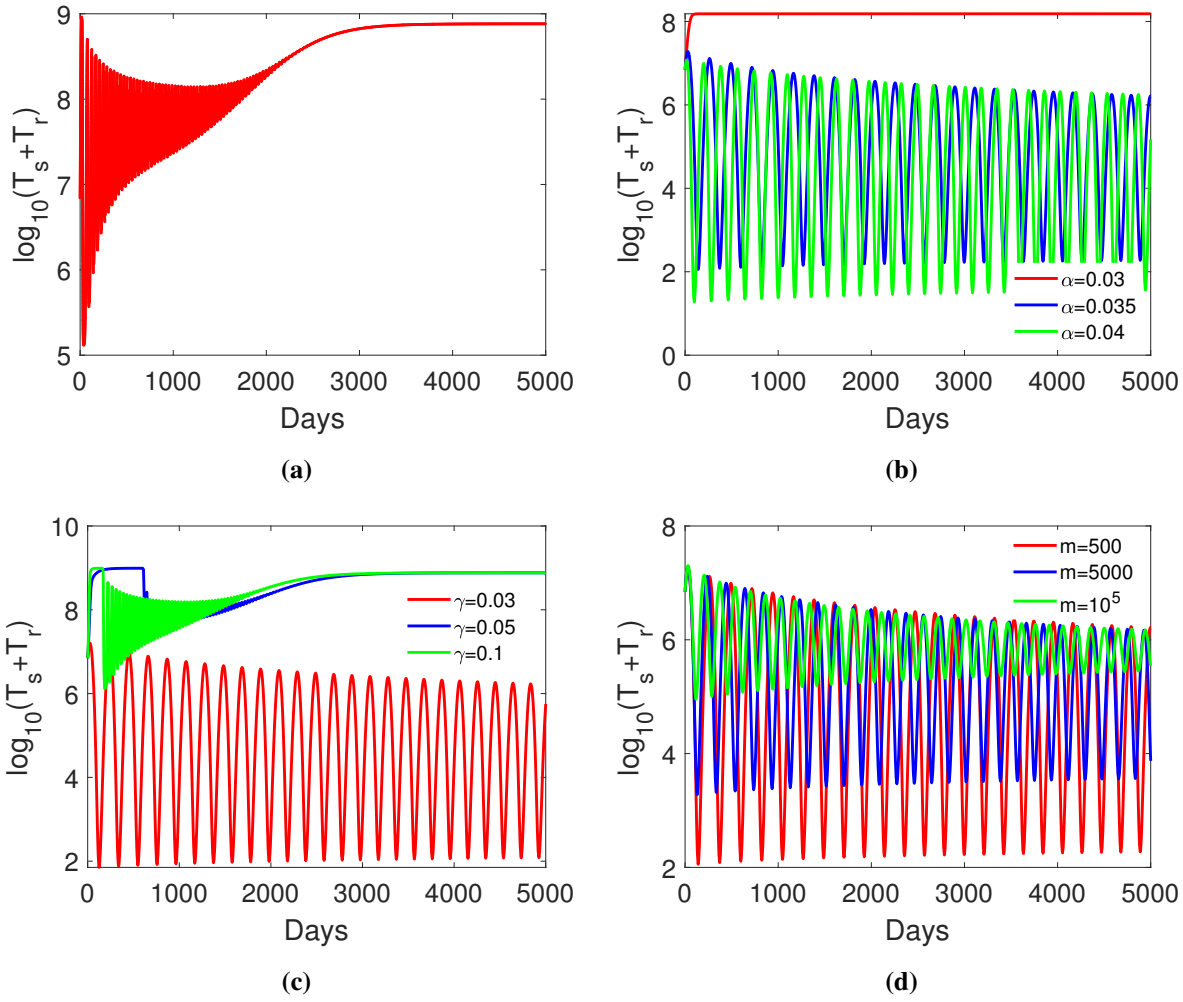

Figure 2. Total tumor load is plotted. (a) The four-dimensional system with no immune cells. Plots (b), (c), and (d) depict the total tumor count of the five-dimensional $T_sT_rT_iVZ$ model with parameter values given in the main text.

In Figure 2(b), the ratio $\dfrac{K}{m+K} = 0.999$, indicating that when $\alpha = 0.03 = \gamma$, the immune system is weak, and the total tumor load is large. As α is increased, the total tumor burden is significantly reduced. This finding is further confirmed by the scenarios shown in plots (c) and (d). Obviously, the solutions of those in Figure 2(b) with $\alpha = 0.03$, and (c) with $\gamma = 0.05$ and 0.1 converge to an equilibrium level. By

utilizing a three-dimensional T_sT_rZ plot, we can determine that the remaining solutions in Figure2(b) with $\alpha = 0.035$ and 0.4 converge to a periodic solution, and so does the solution in (c) with $\gamma = 0.03$. Moreover, each solution presented in (d) also converges to a periodic solution.

Through further adjustments to these parameters, we compared the outcomes and consistently observed that the immune-incorporated system maintained a lower total tumor count compared to the four-dimensional model without immune cells, especially when the recruitment rate of immune cells exceeds the death rate.

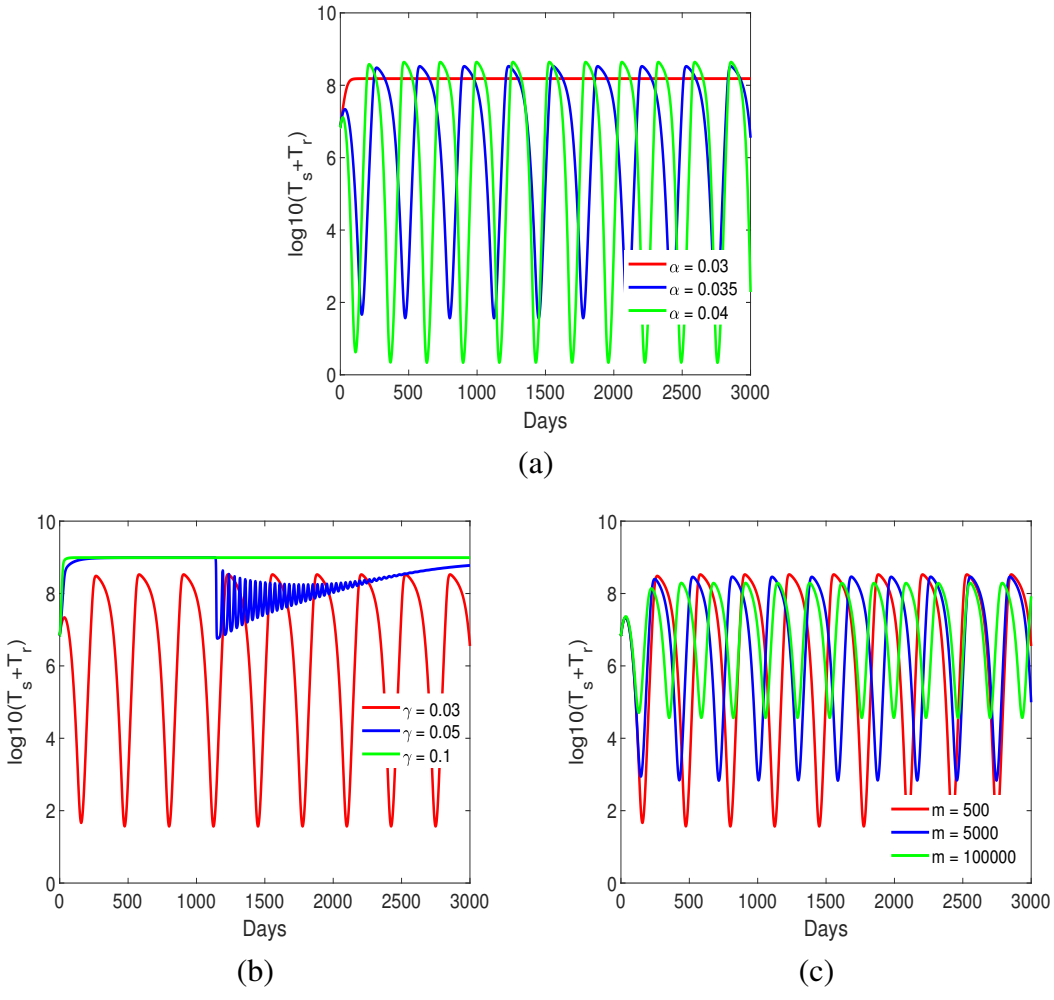

Figure 3. The total tumor load is plotted in plots (a), (b), and (c), depicting the total tumor count of the five-dimensional $T_sT_rT_iVZ$ delay model (2.1) with a delay $\tau = 5$ in immune cell activation and parameter values given in the main text.

Next, we compare the results of the corresponding five-dimensional delay model $T_sT_rT_iVZ$ with the four-dimensional $T_sT_rT_iV$ ODE model, which does not include immune cells. Here, we consider the delay in immune cell activation with $\tau = 5$. In previous results without delay, as shown in Figure 2(b), an increase in the maximal immune cell proliferation rate α visibly lowered the total tumor burden. However, as depicted in Figure 3(a), with a small α value of 0.03 and delay, the stability of the

equilibrium remains unchanged. When α is increased to 0.035, the amplitude of oscillation is larger in the delay model, and the total tumor load may exceed that for $\alpha = 0.03$. A similar phenomenon is observed as α is further increased to 0.04. However, the tumor burden is clearly smaller than that of the model without immune cells.

Regarding the immune cell death rate γ, it is apparent from Figure 3(b) that immune cells are not effective in controlling the tumor if the death rate $\gamma = 0.1$ is large. As γ is reduced to 0.03, it is evident that the immune cells can lower the total tumor load even with a recruitment delay as shown in Figure 3(b). Further, the tumor load attains a larger maximum value with a delay compared to that without delay presented in Figure 2(c). A similar conclusion is also obtained as m is varied. The time delay in immune recruitment can increase the amplitude of the tumor burden.

5.2. Sensitivity analysis

The feasible parameter ranges of the model are compiled from the literature and presented in Table 2. The killing rate k_r of resistant cancer cells by immune cells was estimated over a broader range of 10^{-4}–10^{-2} cell^{-1} day^{-1}, while the killing rate k_s of susceptible tumor cells by immune cells is set at 10^{-5}–10^{-3} cell^{-1} day^{-1}. From the previous subsection, the initial conditions for Eq (2.1) with $\tau = 0$ are set as $(7 \times 10^6, 10^2, 0, 5 \times 10^6, 2 \times 10^3)$. For Eq (2.1) with $\tau > 0$, the history function is set as

$$\phi_1(t) = 7 \times 10^6, \quad \phi_2(t) = 10^2, \quad \phi_3(t) = 0, \quad \phi_5(t) = 2 \times 10^3, \quad t \in [-\tau, 0], \tag{5.1}$$

and

$$\phi_4(t) = 0, \quad t \in [-\tau, 0), \quad \phi_4(0) = 5 \times 10^6. \tag{5.2}$$

In OVT, OVs can be administered following single dose or multiple dose regimens [35]. In this paper, single dose regimens are used, and OVs are administered at time $t = 0$. Population dynamics are solved numerically using the built-in function ode23tb in Matlab for $\tau = 0$, and a history for population levels is created for solving Eq (2.1) with $\tau > 0$.

Sensitivity analysis is a common method used to identify critical inputs in a model. Global sensitivity analysis (GSA) is a method to analyze the impact of each input or parameter on the output uncertainty when all model inputs or parameters change randomly [44]. In this subsection, we conduct GSA utilizing the Partial Rank Correlation Coefficient (PRCC) to assess the relationship between each parameter and tumor size, $T_s + T_r$. Furthermore, GSA aids in selecting parameters for the bifurcation analysis to be performed in the next section. The parameter ranges are shown in Table 2. For the introduction and implementation of this method, we refer to the works by Marino et al. [44] and Vithanage et al. [17, 18].

Table 2. Meanings and plausible ranges of parameters.

Parameter	Description	Range	Reference
K	Carrying capacity of tumor	10^8–9.7×10^9 cells	[19, 22]
r_s	Rate of growth of sensitive tumor cells	0.18–0.97 day^{-1}	[18, 19, 36, 37]
β	Virus transmission rate	6×10^{-12}–0.862 pfu^{-1}day^{-1}	[22, 38]
r_r	Growth rate of resistant tumor cells	$r_s \times$ [0.01 0.97] day^{-1}	[8, 39]
b	Death rate of infected tumor cells	1.333–2.667 day^{-1}	[16]
q	Virus burst size per infected tumor cell	10–1350 pfu cell^{-1}	[16]
c	Viral clearance rate	0.024–24 day^{-1}	[40]
a	Rate of mutation of sensitive cancer cells	10^{-9}–10^{-3} day^{-1}	[12, 41]
d	Rate of transition from resistance to sensitivity	0 – 1 day^{-1}	guess
m	Half-saturation constant of immune cell proliferation rate	40 – 10^5 cells	[16, 22]
γ	Death rate of immune cells	0.024–0.178 day^{-1}	[22]
α	Maximal immune cell proliferation rate	0.024–2.4 day^{-1}	[22]
k_s	Killing rate of susceptible tumor cells	10^{-5}–10^{-3} cell^{-1} day^{-1}	[17]
k_r	Killing rate of resistant tumor cells	10^{-4}–10^{-2} cell^{-1} day^{-1}	guess
k_i	Killing rate of infected tumor cells	9.6×10^{-3}–4.8 cell^{-1} day^{-1}	[16, 22]
k_v	Killing rate of viruses	0.024 – 48 cell^{-1} day^{-1}	[22]
τ	Delay in the activation of immune cells	1–8 days	[42, 43]

According to Liu et al. [45] and De Matos et al. [46], rapid immune-mediated clearance of oncolytic viruses can affect the efficacy of OVT. Following virus administration, oncolytic virus infection and replication within the tumor play a crucial role in the initial days [47, 48]. Selecting $T = 7$ for a short time interval enables the identification of parameters potentially related to the early-stage anti-tumor or anti-viral effects. In contrast, choosing $T = 21$ for a longer time interval helps pinpoint parameters associated with the asymptotic tumor size and the treatment outcome. GSA will be conducted with two endpoints, $T = 7$ and $T = 21$.

In Figure 4, PRCC is computed for each parameter. The criteria for the strength of a correlation in [49] are used in this paper. A correlation is considered non-important if $|\text{PRCC}| < 0.2$, weak if $0.2 < |\text{PRCC}| < 0.5$, strong if $0.5 < |\text{PRCC}| < 0.7$, and very strong if $0.7 < |\text{PRCC}|$. Figure 4(a),(b) depicts the PRCC for each parameter in Eq (2.1) with $\tau = 0$. The maximum immune cell proliferation rate, α, shows a strong negative correlation with the tumor size at $T = 7$. The virus transmission rate, β, exhibits a weak positive correlation with the tumor size when $\tau = 0$. All other parameters show unimportant correlations with the final tumor size.

It has been reported that the activation of the adaptive immune response takes at least several days [43], and Pulendran et al. and Sun et al. have noted that after infection, T lymphocytes go through an expansion phase, reaching their peak on day 8 in response to antigen stimulation [42, 50]. To examine the effect of delay in immune cell proliferation, we choose a larger delay in its range (Table 2). In Figure 4(c),(d), we consider Eq (2.1) with $\tau = 7$. The maximum immune cell proliferation rate, α, and the killing rate, k_s, have strong negative correlations with the tumor size at $T = 7$. All other parameters show weak or unimportant correlations with the final tumor size.

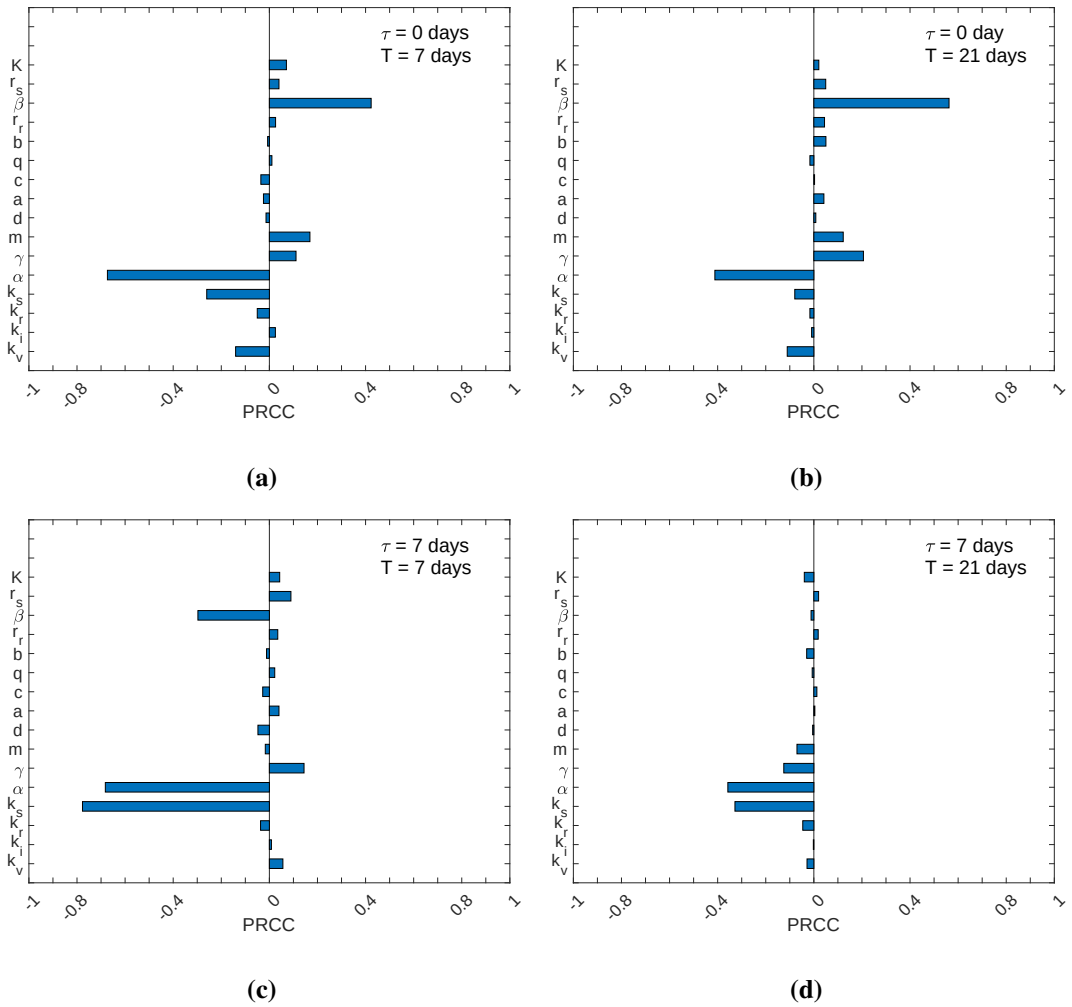

Figure 4. Global sensitivity analysis based on Table 2. Initial conditions are the same as in Eqs (5.1) and (5.2). The PRCC between each parameter and the final tumor size, $T_s(T)+T_r(T)$ at the endpoint T is shown in panels (a) and (b) for $\tau = 0$ and panels (c) and (d) for $\tau = 7$.

Figure 4 shows consistency of important parameters in all cases. Parameters α and k_s related to immune cell proliferation and immune response have strong correlations with the tumor size. We explore the correlations by studying the tumor dynamics, $T_s(t) + T_r(t)$ for $0 \le t \le 21$, with selected parameter values for α, k_s, and β. All other parameter values are fixed as follows:

$$K = 10^9, r_s = 0.45,\ r_r = 0.3,\ b = 1.33,\ a = 0.01,\ c = 1.83,\ \gamma = 0.17,\ m = 10^5, \tag{5.3}$$

$$d = 0.1,\ \beta = 10^{-6},\ q = 10^2,\ \alpha = 0.2,\ k_r = 10^{-4},\ k_s = 10^{-5},\ k_i = 1.8,\ k_v = 0.15. \tag{5.4}$$

Figure 5(a),(d) shows the tumor dynamics $T_s + T_r$ for selected α values. Larger proliferation rates result in smaller tumor sizes. Equation (2.1) models a delay in immune cell proliferation. Figure 5(d) shows a delay in tumor cell elimination compared with Figure 5(a), which reflects a delay in immune cell proliferation. Figure 5(b),(e) shows larger tumor killing rates, k_s, resulting in smaller tumor sizes. Interestingly, Figure 5(b),(e) suggests that the killing rate, k_s, must exceed 5×10^{-4} to effectively destroy

the tumor cells. Hale et al. have reported that the immune response is important for the success of treatment and preventing tumor recurrence [51].

Figure 5(c),(f) shows the same tumor dynamics when $\beta < 10^{-6}$, implying that the virus transmission rate is insufficient to induce an anti-tumoral effect if $\beta < 10^{-6}$. In contrast, the tumor population drops dramatically initially when $\beta = 10^{-4}$ and $\beta = 10^{-3}$, indicating that tumor cells are infected after viruses are administered. As the virus transmission rate increases, more tumor cells are infected, leading to a smaller population level of $T_s + T_r$. The tumor size for $\tau = 7$ is slightly smaller than that for $\tau = 0$, implying that a delay in immune cell proliferation may reduce anti-viral response. Based on the above numerical result, we assume $\beta \geq 10^{-6}$ from this point onward.

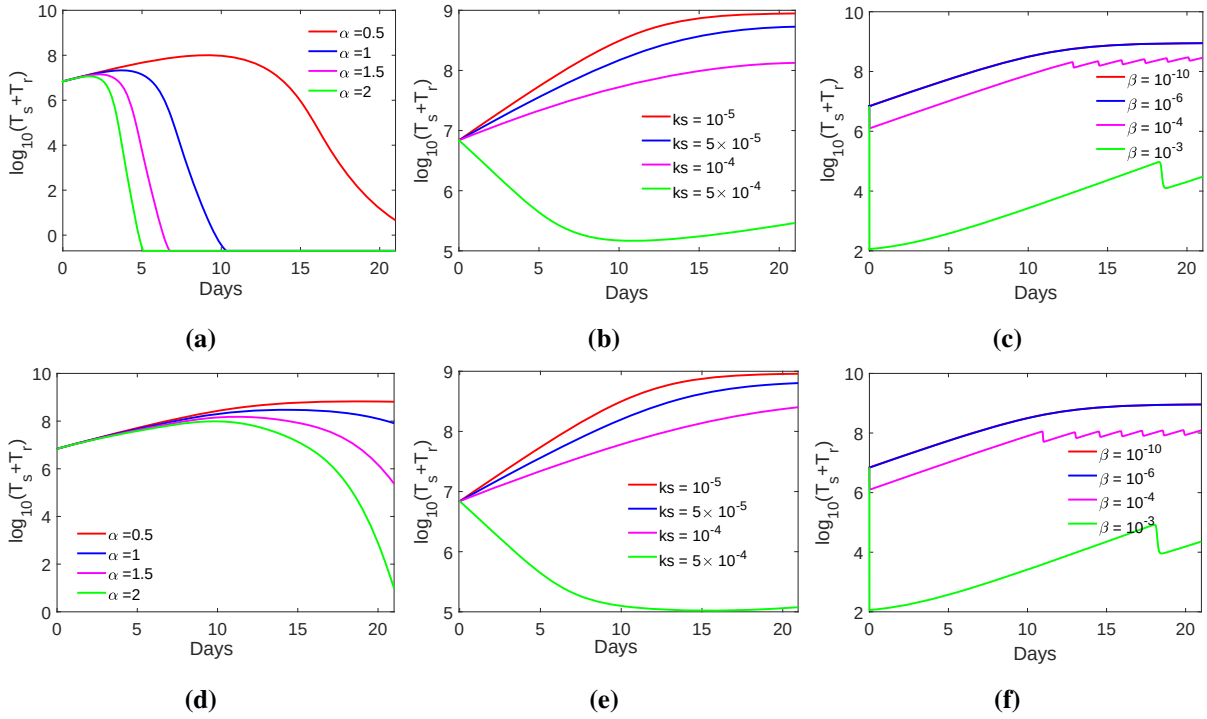

Figure 5. The tumor size $T_s(t) + T_r(t)$ for $0 \leq t \leq 21$ at various parameter values for α, k_s, and β which have strong correlations with the tumor size. (a) $\tau = 0$, (b) $\tau = 0$, (c) $\tau = 0$, (d) $\tau = 7$, (e) $\tau = 7$, and (f) $\tau = 7$.

5.3. Numerical methods for bifurcation analysis

Bifurcation analysis is the study of changes in the asymptotic behavior of a model under parameter variation and can provide a complete picture of asymptotic dynamics on a parameter domain. Bifurcation analysis usually begins with the identification of equilibria. Given a set of parameter values, the numerical method constructed in [18] can be directly applied to locate the equilibrium E_2 and all positive equilibria. The mathematical analysis given in Section 3 can be used to find all other boundary equilibria. The numerical method in [52,53] is then applied to compute the bifurcations of equilibria. To study the effect of OVT, the virus transmission rate β is used as a bifurcation parameter. Note that Figure 5(c),(f) shows that the virus transmission rate β must be greater than 10^{-6}. We use the range $[10^{-6}, 1]$ for β. From GSA, the immune response is an important factor associated with the tumor size. The

half-saturation constant, m, of the immune cell proliferation rate measures the steepness of the curve for the activation of immune cells in response to the presence of tumor cells. A small half saturation constant results in a sharp increase in immune cells with increasing tumor cells. We use m as the other bifurcation parameter.

Mahasa et al. [16] have suggested a half saturation constant of 40 cells in their model. The term describing immune cell proliferation in their model is independent of immune cells. With such a small half-saturation constant in Eq (2.1), immune cell proliferation is almost constant in the presence of tumor cells. The process of activation of immune cells involves the interaction between tumor cells and APCs (antigen presenting cells) [54]. Once activated, CD8+ T cells undergo clonal expansion with interleukin-2 (IL-2) stimulation [55]. Based on the biological mechanism of the activation and expansion process, the immune cell proliferation term in the fifth equation of the ODE system is modeled as a function of both tumor cells and immune cells. To match a similar proliferation rate in the model by Mahasa et al. [16], the half-saturation constant m may be a large number. Storey et al. [22] has suggested a range of $40 - 10^5$ cells for m based on the work by Banerjee et al. [56]. The model considered in [56] does not consider a half saturation constant in the recruitment term for immune cells. Thus, the range of the half-saturation constant, m, has not been validated or justified in these works [16, 22, 56].

It has been shown that a small half-saturation constant may cause destabilization and produce sustained oscillations in population sizes [57–59]. Incorporating a delay in the ODE system can also lead to population oscillations in the solution. Using a range of small half-saturation constants may hinder the study of the destabilization effect caused by the time delay. Furthermore, as pointed out above, the half-saturation constant m may be a large number, and it affects the tumor size in the equilibria. Therefore, we use a wide range for m. Let $[10^{-6}, 1] \times [10^5, 10^9]$ be the parameter domain for β and m. Other parameters are fixed as in Eqs (5.3) and (5.4). An adaptive grid method in Section 2.1 in [52] is applied with a 10 by 10 grid in the parameter domain. The regions containing bifurcation curves are refined with 6 levels. The code is implemented in Matlab, where the Newton method is used to find the equilibrium that has no analytic solution, and the built-in function eig is used to solve the eigensystem of the Jacobian matrix. The bifurcation diagram is shown in Figure 6(a).

All six equilibria coexist in a region of the parameter domain. Proposition 3.3 has shown that the tumor-free equilibrium E_0 is unstable. From Eqs (3.2), (5.3) and (5.4), along with Proposition 3.3, the equilibrium E_1 is unstable in the parameter domain (Figure 6(a)). The numerical simulation agrees with Proposition 3.3. There are one saddle node bifurcation curve SN, one Hopf bifurcation curve $Hopf_0$, and two transcritical bifurcation curves Tr_1 and Tr_2. Both positive equilibria appear through saddle-node bifurcations on the curve SN. We use the notation E_{41} for the positive equilibrium that might be stable. The equilibrium E_{42} is never stable. The positive equilibrium E_{41} changes its stability through Hopf bifurcations on the curve $Hopf_0$ when $\tau = 0$. Other bifurcations such as bifurcations of limit cycles may occur in the parameter domain. These bifurcations do not affect the stability property of the equilibria shown in Figure 6(a) and are out of the scope of this paper. Therefore, they will not be studied in this paper. The positive equilibria E_{41} loses its stability through transcritical bifurcations, Tr_2, and the equilibrium E_3 becomes stable when m increases. Note that the region above Tr_2 satisfies the condition in Eq (3.20), and the curve Tr_2 satisfies the condition $a_{55} = 0$ in Eq (3.20). The equilibrium E_2 is stable when (β, m) lies below the transcritical bifurcation curve Tr_1 for $\tau = 0$, and it is unstable when (β, m) lies above Tr_1. Our numerical computation agrees with Proposition 3.5. The conditions Eqs (3.11) and (3.16) are satisfied in the region where E_2 is stable, and the curve Tr_1 satisfies the left hand

side of Eq (3.16) equal to zero. Our numerical computation agrees with Proposition 3.6. Bistability exists in a region below Tr_1.

Consider Eq (2.1) with $\tau > 0$. Recall that ODE and DDE systems have the same equilibria. The local stability of an equilibrium depends on the signs of the real parts of the solutions to $det(A-\lambda I+Be^{-\lambda\tau}) = 0$, where A and B are defined in Section 4.2. If $\lambda = 0$ is a solution to $det(A - \lambda I + Be^{-\lambda\tau}) = 0$, it is also a solution to $det(A + B - \lambda I) = 0$. System (2.1) goes through the same bifurcations as the ODE system does on the bifurcation curves SN, Tr_1, and Tr_2. It is known that incorporating a time delay τ into the ODE system may produce destabilization effects and cause fluctuations in population dynamics through Hopf bifurcations [60]. A numerical method is proposed to identify such Hopf bifurcations for system (2.1) in a parameter domain when τ is fixed.

Based on the bifurcation curves for $\tau = 0$ shown in Figure 6, we focus on the Hopf bifurcations for system (2.1) in the region where E_{41} is stable. At a Hopf bifurcation of E_{41} for $\tau > 0$, $det(A-\lambda I+Be^{-\lambda\tau}) = 0$ has a pair of pure imaginary roots. All other solutions have negative real parts. Starting with any Hopf bifurcation point on $Hopf_0$, say (β_0, m_0), let $\pm i\omega_0$ be the pure imaginary eigenvalues for $A + B$. We fix β_0 and use ω_0 and m_0 as an initial guess to find ω and m for a Hopf bifurcation point of system (2.1) with a fixed $\tau > 0$. It may be assumed that all other solutions of $det(A - \lambda I + Be^{-\lambda\tau}) = 0$ at the parameter point (β_0, m) have negative real parts. Otherwise, another bifurcation curve other than $Hopf_0$, SN, Tr_1, and Tr_2 would appear in Figure 6(a). It is worth noting that ω and m appear in several entries of the matrix $A - i\omega I + Be^{-i\omega\tau}$. The Newton method is not practical since it involves taking derivatives with respect to ω and m. In this paper, the Nelder-Mead simplex method [61], which is a direct method, is employed for finding ω and m. The detailed algorithm can be found in [61], or the built-in function "fminsearch" in Matlab can be directly applied for this purpose.

Mahasa et al. [16] studied a mathematical model of OVT with a time delay in the stimulation of virus-specific immune cells. The time delay τ in their work was fixed at 7 hours, and their work showed that the time delay $\tau = 7$ hours does not affect the stability of the virus-free equilibrium. In this work, we use $\tau = 1$ day and $\tau = 7$ days, which are at both ends of the parameter range shown in Table 2. When (β_0, m) is not close enough to (β_0, m_0), the continuation technique with some smaller increments in τ helps with the success of identifying m for $\tau = 1$. With each point on $Hopf_0$ as an initial guess for the corresponding point on $Hopf_1$, parallel computation helps accelerate the process. Hopf bifurcation curves $Hopf_1$ with $\tau = 1$, $Hopf_2$ with $\tau = 1$, and $Hopf_3$ with $\tau = 7$ are computed and shown in Figure 6(b). The equilibrium E_{41} changes its stability on the curves $Hopf_1$ and $Hopf_3$ when $\tau = 1$ and $\tau = 7$, respectively. The curve $Hopf_3$ is above $Hopf_1$ which is above $Hopf_0$, indicating that the presence of time delay destabilizes the system. For Eq (2.1) with $\tau = 1$, the curve $Hopf_2$ shows Hopf bifurcations where E_2 changes its stability. The equilibrium E_2 is stable in the region bounded by the curves Tr_1 and $Hopf_2$. This shows again time delay exhibits a destabilization effect in Eq (2.1). Theorem 4.2 gives a condition for the stability of E_2 when $\tau > 0$. The stability condition is given in Eq (4.12). Equation (4.12) is independent of β. Therefore, we examine the condition with the parameter values used in Figure 6. According to Theorem 4.2, the equilibrium E_2 is stable for $\tau > 0$ when $m > 1.208 \times 10^7$. We then use the numerical method proposed in this section to compute the Hopf bifurcation for E_2 for $\tau < 1000$ and find that E_2 is stable when $m > 1.205 \times 10^7$ for $\tau < 1000$. Our numerical computation agrees with Eq (4.12). Since such large τ values are not within the plausible range of τ, the figure is not shown in this paper.

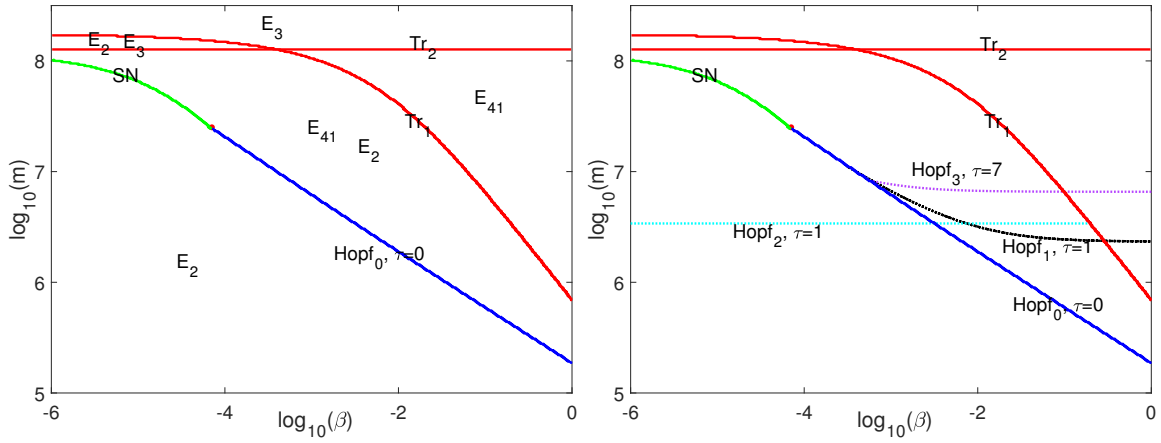

(a) **(b)**

Figure 6. Bifurcation diagram using β and m as bifurcation parameters and Eqs (5.3) and (5.4) for all other parameters. (a) Regions where the equilibria are stable. (b) Hopf bifurcation for selected τ values to show the destabilization effect of time delay. The red curves represent transcritical bifurcations (Tr), the green curve represents saddle-node bifurcations (SN), and the rest of the curves represent Hopf bofurcations (Hopf).

5.4. Virus transmission rate and the steepness of immune cell proliferation

In this subsection, we study the effect of virus transmission rate β and the steepness of immune cell proliferation m on the outcome of treatment. Let $\beta = 0.1$, which corresponds to a relatively large virus transmission rate for the range of β in Table 2. Let $m = 2 \times 10^6$. Note that this set of parameter values lies in the region where both E_2 and E_{41} are stable, as shown in Figure 6(a). The tumor persists with a population size of $T_s + T_r + T_i = \gamma m/(\alpha - \gamma)$. Furthermore, the tumor-free equilibrium E_0 is unstable, meaning that either the treatment may fail or tumor relapse may occur. This simulation can help identify factors that may cause unsuccessful treatment or tumor recurrence and further help design strategies to improve OVT treatment.

Consider the initial condition $(7 \times 10^6, 100, 0, 5 \times 10^6, 2 \times 10^3)$ for treating a tumor of 7×10^6 cells with a therapeutic dose of 5×10^6 pfu. Figure 7(a) shows that the population dynamics approach the stable equilibrium E_{41}. The stability of E_{41} implies that the virus is persistent. Virus persistence has been observed in experimental studies and proven as a means to slow down tumor growth [62]. The sensitive tumor cells (red curve) are infected quickly after the treatment, and thus the infected tumor cells (black curve) increase rapidly. The tumor cells respond to the treatment initially but develop resistance to the therapy causing an increase in resistant tumor cells (blue curve). Note that the elimination of resistant tumor cells relies on immune cells (green curve), and the immune system is not able to control the resistant tumor cells. Strategies to reduce resistant tumor cells or enhance the immune response to resistant tumor cells are required to overcome this challenge.

Let $\tau = 1$, and all parameter values remain the same as used for Figure 7(a). Figure 7(b) shows population oscillations. The equilibrium E_{41} becomes unstable, demonstrating the destabilization effect caused by time delay. A slightly larger m value is used with $\tau = 1$ and $\tau = 7$. Let $m = 3 \times 10^6$. The equilibrium E_{41} is stable when $\tau = 1$ and unstable when $\tau = 7$, where the population dynamics are

similar to the population dynamics in Figure 7(a),(b), respectively. Equation (2.1) with $\tau > 0$ exhibits a destabilization effect. Treatment is not successful in either case, $\tau = 0$ or $\tau > 0$.

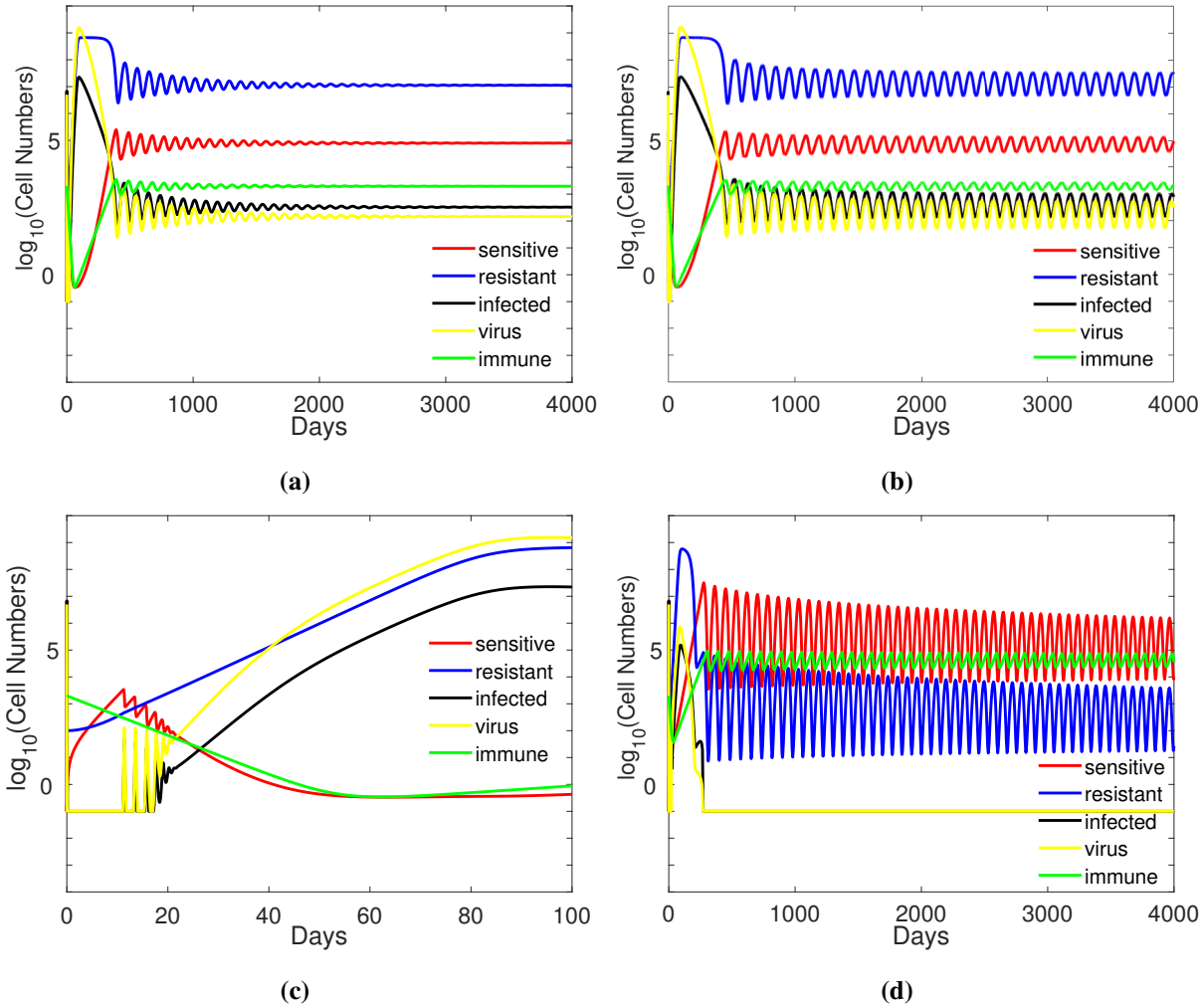

Figure 7. Population dynamics for (a) $\beta = 0.1$, $m = 2 \times 10^6$, $\tau = 0$, (b) $\beta = 0.1$, $m = 2 \times 10^6$, $\tau = 1$, (c) a magnification of part (a) for $t \in [0, 100]$, and (d) $\beta = 0.1$, $m = 10^4$, $\tau = 0$. All other parameter values are kept the same as in Eqs (5.3) and (5.4), and initial conditions are the same as in Eqs (5.1) and (5.2).

Figure 7(a),(b) shows that the OVT is effective initially when the transmission rate $\beta = 0.1$, where the susceptible tumor cells are infected and killed. The immune cells go through the contraction phase after eliminating the infected cells. However, part of the susceptible tumor cells develop resistance to treatment, as shown in Figure 7(c), which presents a closer look at Figure 7(a). The resistant tumor population grows progressively, and the treatment ultimately fails. Consider $m = 10^4$, which corresponds to a quicker immune cell proliferation in response to tumor growth. Figure 7(d) shows that a quicker immune response eliminates infected cells and viruses but not the other two populations of tumor cells. The anti-viral response, where viruses are cleared by the immune system, is a challenge in OVT [45, 46]. Furthermore, a low half-saturation constant tends to cause an oscillation of populations [57, 58].

Such persistent large scale oscillations are unlikely to be seen in tumor immune interactions [63]. Nevertheless, oscillations in tumor and immune cell populations may account for the transitional state between elimination and equilibrium phases in immunoediting [63].

Let $\beta = 10^{-6}$, which corresponds to a small virus transmission rate compared with the previous simulation. Let $m = 2 \times 10^6$. Figure 8 shows that the OVT is ineffective when the virus transmission rate β is small. The infected tumor cell population is small and eliminated soon, but the immune system is not able to eliminate the other two populations of tumor cells. This result agrees with the result shown in Figure 5(c),(f). Again, a quicker immune response by using a smaller half saturation constant m or a time delay $\tau > 0$ does not improve the outcome of OVT but causes an oscillation of populations. The figures are not shown here as the population dynamics are similar to those in Figure 7(d).

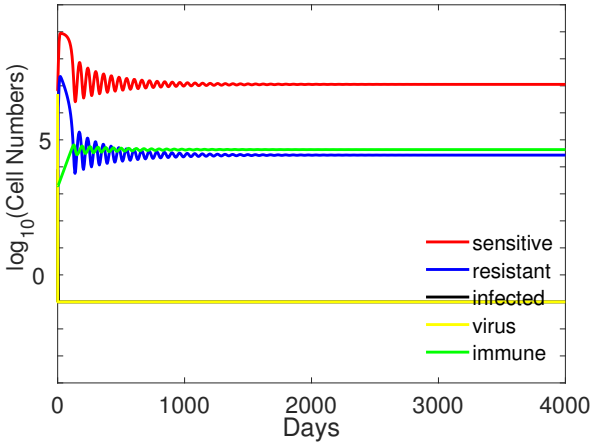

Figure 8. Population dynamics for $\beta = 10^{-6}$, $m = 2 \times 10^6$, $\tau = 0$. All other conditions are the same as in Figure 7.

It is known that the interactions between the immune system and oncolytic viruses, resulting in both anti-viral and anti-tumoral responses, can have both beneficial and detrimental effects on the outcome of OVT [3,45,64]. Several studies have suggested the use of combination therapy with other immunotherapeutic approaches to improve the efficacy of treatment [64–66]. Guedan and Alemany [67] have published a review article addressing the potential role of combination therapy using OVT and CAR T-cell therapy in fighting cancer. It is expected that combination therapy using OVT and CAR T-cell therapy can improve the outcome of the OVT studied in this subsection.

5.5. Combination therapy using OVT and CAR T-cell therapy

Chimeric antigen receptor T-cell (CAR T-cell) immunotherapy is a novel revolutionary cancer treatment. The process of CAR T-cell therapy involves deriving T cells from the patient and engineering these T cells *in vitro* to promote the recognition of cancer cells and improve T-cell function. CAR T cells are then expanded and infused back into the patient to enhance the elimination of tumor cells [68–70]. Preclinical studies in combination therapies of OVT and CAR T-cell therapy have been conducted to investigate the synergistic effects [71], and the results have shown sustained anti-tumor immune response yielding promising treatment outcomes [72].

According to Figure 5 (c),(d), the killing rate must be at least 5×10^{-4} to effectively fight tumor cells.

From Section 5.4, the development of resistance to OV is a challenge to the success of OVT. Assume that the engineered T cells have higher killing rates of susceptible and resistant cells than used in Section 5.4. Let $k_s = 5 \times 10^{-4}$, $k_r = 5 \times 10^{-3}$. Consider $\beta = 0.1$, and $m = 2 \times 10^6$. Gruber et al. studied the relationship between tumor cells and T lymphocytes in breast cancer patients, and the patients had CTL counts of 365 ± 194 cells/μL (Mean ± SD) [73]. Within two standard deviations of the mean, it is safe to say that CTL counts for most patients range from several tens to 750 cells/μL. The dose levels for CAR T-cell therapy are reported to range from 60 million to 600 million cells [74, 75]. For a person with body weight of 70 kg, about 7.2 percent of body weight is blood [76]. That is about 5 liters of blood. The concentration of CAR T cells in blood is about 12–120 cells/μL. The goal of CAR T cell therapy is to generate a sufficient number of CAR T cells to go into the tumor site to effectively target and attack the cancer cells [77]. From the simulation in the previous section, the numbers of effector cells in the stable equilibria E_2 (Figure 8) and E_{41} (Figure 7(a)) are 43,000 and 2000, respectively. In this example, we simulate the concurrent administration of both agents. Using the initial condition $(7 \times 10^6, 100, 0, 5 \times 10^6, 8000)$, where the number of the initial immune cells is 8000, Figure 9(a) shows that combination therapy is able to eradicate tumor cells. After the elimination of tumor cells, the immune cells go through the contraction phase. Further simulation shows that monotherapy using either CAR T-cell immunotherapy ((Figure 9(b)) or OVT (Figure 7(a)) is not able to eliminate the tumor. It has been reported that CAR T cell therapy is ineffective for solid tumors [77]. Combination therapy produces a synergistic effect [72].

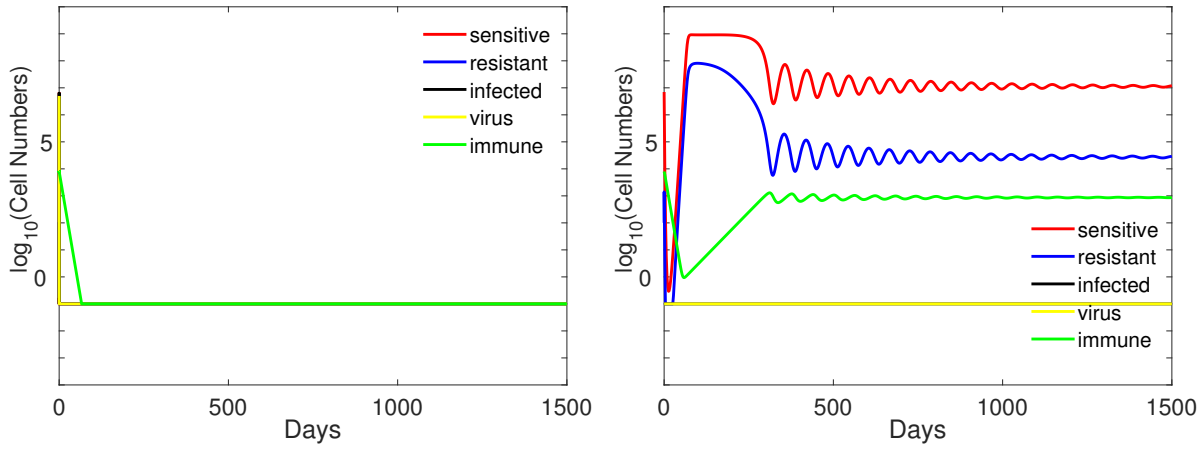

Figure 9. (a) Population dynamics for $\beta = 0.1$, $m = 2 \times 10^6$, and $\tau = 0$. All other parameter values are kept the same as in Eqs (5.3) and (5.4) except for $k_s = 5 \times 10^{-4}$ and $k_r = 5 \times 10^{-3}$. The initial conditions are $(7 \times 10^6, 100, 0, 5 \times 10^6, 8000)$. (b) Monotherapy using CAR T cell therapy.

Consider a larger tumor with 10^9 cells, which corresponds to a tumor of approximately 1 cm in diameter [34]. It is known that virus clearance mediated by innate and adaptive immune cells is a significant challenge in OVT [78]. The innate immune response acts rapidly [79, 80]. We use time delay to simulate the strategy to circumvent this virus clearance in the initial days. Fu et al. [62] conducted experiments to show that genetically coating oncolytic virus with CD47 allows OVs to evade the immune

response and promotes virus persistence at the tumor site. We use a lower k_v value to simulate evasion of the immune response and to enhance virus persistence. Let $k_v = 0.03$ in this simulation. Figure 10(a) shows that the combination treatment is successful with a low dose of 5000 CAR T cells, compared with the simulation in Figure 9(a). The results of further simulation of other cases are summarized in Table 3. Combination therapy allows the use of lower doses of each agent and achieves better efficacy. According to Eldar-Boock et al. [81], combination therapy can reduce the toxicity and side effects due to lower doses.

Table 3. Efficacy of different combination treatments. Efficacy is measured by the largest tumor size for which the treatment is successful. Ineffective means that the treatment is unable to eradicate a tumor of 7×10^6 cells. The notation CD7 represents the strategy to enhance virus persistence. Time delay $\tau > 0$ represents the strategy to evade virus clearance in the initial days.

Therapy Strategy	Delay $0 \le \tau \le 7$	Number of CAR T cells	Efficacy Number of Tumor cells
OVT	$\tau \ge 0$	—	Ineffective (Figures 7 and 8)
CAR T cell	$\tau \ge 0$	8000	Ineffective (Figure 9(b))
CAR T cell+OVT	$\tau = 0$	8000	10^8
CAR T cell+OVT	$\tau \ge 4$	5000	10^9
CAR T cell+OVT+CD7	$\tau = 0$	8000	10^9
CAR T cell+OVT+CD7	$\tau \ge 4$	5000	10^9

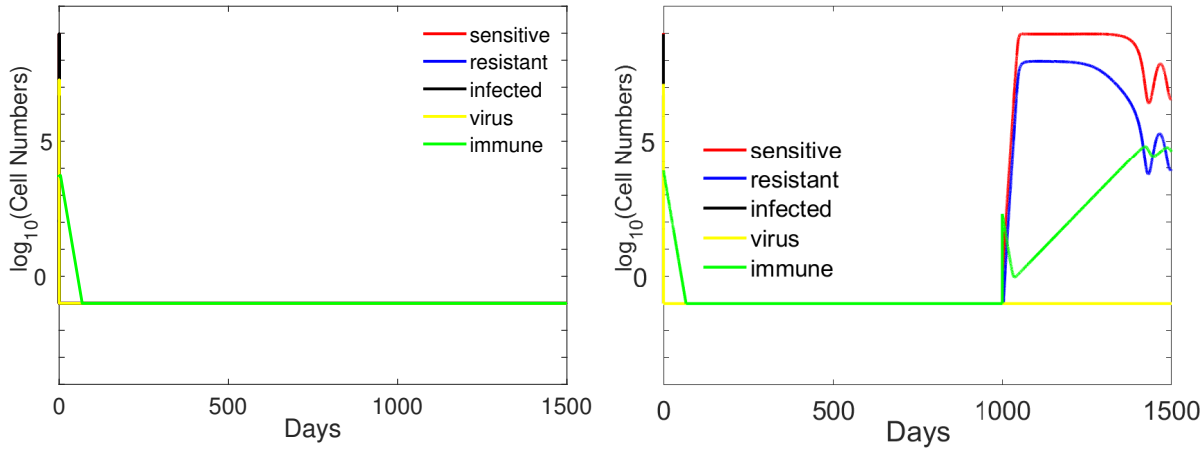

Figure 10. (a) Population dynamics for $\beta = 0.1$, $m = 2 \times 10^6$, and $\tau = 4$. All other parameter values are kept the same as in Eqs (5.3) and (5.4) except for $k_s = 5 \times 10^{-4}$, $k_r = 5 \times 10^{-3}$, and $k_v = 0.03$. The initial conditions are $(10^9, 100, 0, 5 \times 10^6, 5000)$. (b) The same simulation as part (a) for $t \in [0, 1000]$. If one tumor cell is formed, say at $t = 1000$, tumor recurrence will occur.

Recall that E_0 is unstable. This implies a small perturbation may cause population dynamics to move away from E_0. In Figure 10(b) we simulate that one susceptible cell is formed at $t = 1000$. Note that 5–10% of T cells become memory T cells during the contraction phase [82, 83]. These memory T cells can quickly respond to previously encountered pathogens [82]. The number of immune cells increases in response to the presence of tumor cells. However, the immune cells cannot control the growth of tumor cells leading to tumor recurrence. It has been reported that tumor recurrence is a formidable challenge for cancer treatment [84].

6. Conclusions

Drug resistance is a common phenomenon encountered in cancer therapy, posing a critical barrier that requires urgent overcoming. The issue of viral resistance is also encountered in oncolytic viral therapy. While various mathematical and computational models that have appeared in the literature focus on investigating resistance to chemotherapy, only one article [15] employs differential equations to address resistance in OVT.

In this study, we extended the work of [15] by incorporating immune cells into the tumor-virus interaction. These immune cells have the capability to eliminate both tumor cells and viruses. We established the existence and stability of boundary equilibria and presented global stability results. We proved that the delay in immune cell recruitment cannot destabilize boundary equilibria in which immune cells are not present. For those boundary equilibria with the presence of immune cells, we provided sufficient conditions based on model parameters for which the delay has no destabilization effects. Additionally, we derived a critical delay value, under which a boundary equilibrium with the presence of immune cells is destabilized when the delay passes through this critical value, leading to tumor oscillations. The introduction of immune cells results in an additional virus-free equilibrium when the recruitment rate of immune cells is sufficiently high. At this virus-free equilibrium, the total tumor burden is smaller compared to the virus-free equilibrium without immune cells. Consequently, we conclude that immune cells can effectively reduce the tumor load under conditions of sufficient immune strength. We also demonstrated numerically, using reasonable parameter values in Section 5.1, that the inclusion of immune cells can lower the tumor burden compared to the model where immune cells are not included.

GSA showed that the virus transmission rate β and the parameters associated with immune response, such as immune cell proliferation rate α and tumor killing rate k_s, were important factors that affected the final tumor population (Figure 4). Strengthening the immune system is crucial for treatment success and preventing tumor recurrence [51]. The numerical simulation demonstrated that the virus transmission rate must exceed a certain threshold to induce an anti-tumoral effect (Figure 5(c),(f)). A numerical method of Hopf bifurcations was developed for system (2.1) with a time delay. Bifurcation analysis (Figure 6), using the virus transmission rate and the half-saturation constant of immune cell proliferation rate as bifurcation parameters, showed that the system (2.1) exhibited rich dynamics. The results of bifurcation analysis agreed with the mathematical analysis in Sections 3 and 4. The time delay τ in the activation of immune cells had a destabilization effect (Figures 6 and 7(a)–(d)).

Numerical simulation showed that the OVT was effective if the virus transmission rate was sufficiently high; however, the treatment may ultimately fail due to the development of resistance (Figure 7(c)). Resistance to oncolytic viruses has been reported to jeopardize the success of treatment [4]. Another

simulation for a lower virus transmission rate showed that the viruses were cleared out before susceptible cells were infected (Figure 8), and thus the OVT was ineffective. Virus clearance is known to be a challenge in OVT [45,46]. Literature has suggested that OVT as monotherapy frequently fails to control tumor progression and sustain a reduction in tumor masses due to anti-viral effect or development of resistance [3, 45, 64, 85]; combination therapy is a preferable solution to overcome such challenges [65, 67, 86, 87].

To enhance the success of treatment, combination therapy using OVT and CAR T-cell therapy was considered in this paper. Numerical simulation showed that the combination therapy produced synergistic effects and enhanced the success of treatment (Figure 9(a)). Monotherapy using either OVT or CAR T-cell therapy is ineffective (Table 3). Further simulation studied treatment strategies to improve the outcome of treatment (Table 3). Circumventing immune clearance of OVs in the initial days allowed the use of a lower dose of CAR T cells and concurrently promoted the efficacy of the combination therapy. This agrees with the viewpoint of experimental and clinical reports. Virus infection and replication during the initial days of OVT significantly impact its efficacy. [47, 48]; one goal of combination therapy is to improve efficacy while reducing toxicity [81]. Additional simulation showed that Prolonged virus persistence enhanced the outcome of treatment, which agreed with the experimental report that prolonging virus persistence improved the efficacy of OVT [62].

Finally, our simulation showed that cancer recurrence occurred after a tumor cell was formed (Figures 10(b)). Evidence has suggested that cancer recurrence has been a major challenge after the initial treatment response [88]. Our simulation results agreed with clinical and experimental research studies. It is expected that these results can be applied to clinical practice. Further studies including clinical tests are needed to further verify these results.

The immune cell assumptions made in this work were simplified. In future research, we intend to introduce more complexity into the interaction. We propose segregating them into two groups: tumor-specific immune cells and virus-specific immune cells. Tumor-specific immune cells will be activated by both resistant and sensitive tumor cells, capable of targeting and eliminating both types of cancer cells. On the other hand, virus-specific immune cells will be recruited by infected tumor cells and viruses, focusing solely on eliminating infected tumor cells and viruses. This revised model will encompass six nonlinear ordinary differential equations. Furthermore, we may introduce time delays, either in the viral cycle or in immune cell recruitment, to further enhance the model's accuracy.

Use of AI tools declaration

The authors declare they have not used AI tools in the creation of this article.

Acknowledgments

We appreciate all four reviewers for their valuable suggestions, which have significantly improved the paper. The research of Hsiu-Chuan Wei was partially supported by the National Science and Technology Council of Taiwan under the grant NSTC 112-2115-M-035-006. The work of S. Jang was partially supported through Travel Support for Mathematicians from the Simons Foundation under MPS-TSM-00002532.

Conflict of interest

The authors declare there is no conflict of interest.

References

1. H. Dong, S. Markovic, *The Basics of Cancer Immunotherapy*, Springer, 2018.
2. R. A. Weinberg, *The Biology of Cancer*, 2^{nd} edition, Garland Science: London, UK, 2013.
3. G. Marelli, A. Howells, N. R. Lemoine, Y. Wang, Oncolytic viral therapy and the immune system: A double-edged sword against cancer, *Front. Immunol.*, **9** (2018), 1–9. https://doi.org/10.3389/fimmu.2018.00866
4. M. Noll, S. Berchtold, J. Lampe, N. P. Malek, M. Bitzer, U. M. Lauer, Primary resistance phenomena to oncolytic measles vaccine viruses, *Int. J. Oncol.*, **43** (2013), 103–112. https://doi.org/10.3892/ijo.2013.1914
5. M. Bodnar, U. Forys, Modeling of drug resistance: Comparison of two hypotheses for slowly proliferating tumors on the example of low-grade gliomas, *Math. Methods Appl. Sci.*, **45** (2022), 4161–4184. https://doi.org/10.1002/mma.7893
6. M. Becker, D. Levy, Modeling the transfer of drug resistance in solid tumors, *Bull. Math. Biol.*, **79** (2017), 2394–2412. https://doi.org/10.1007/s11538-017-0334-x
7. M. Bodnar, U. Forys, Two models of drug resistance for low grade gliomas: Comparison of the models dynamics, in *Proceedings of the XXII National Conference on Mathematics Applied in Biology and Medicine*, (2017), 37–42.
8. A. Denes, S. Marzban, G. Rost, Global analysis of a cancer model with drug resistance due to Lamarckian induction and microvesicle transfer, *J. Theor. Biol.*, **527** (2021), 110812. https://doi.org/10.1016/j.jtbi.2021.110812
9. J. M. Greene, S. Sanchez-Tapia, E. D. Sontag, Mathematical details on a cancer resistance model, *Front. Bioeng. Biotechnol.*, **8** (2020), 501. https://doi.org/10.3389/fbioe.2020.00501
10. I. Kareva, Different costs of therapeutic resistance in cancer: Short- and long-term impact of population heterogeneity, *Math. Biosci.*, **352** (2022), 108891. https://doi.org/10.1016/j.mbs.2022.108891
11. K. Bao, An elementary mathematical modeling of drug resistance in cancer, *Math. Biosci. Eng.*, **18** (2021), 339–353. https://doi.org/10.3934/mbe.2021018
12. D. K. Bhatt, T. Janzen, T. Daemen, F. J. Weissing, Modelling the spatial dynamics of oncolytic virotherapy in the presence of virus-resistant tumour cells, *PLoS Comput. Biol.*, **18** (2022), e1010076. https://doi.org/10.1371/journal.pcbi.1010076
13. D. K. Bhatt, R. Chammas, T. Daemen, Resistance mechanisms influencing oncolytic virotherapy, a systematic analysis, *Vaccines*, **9** (2021), 1166. https://doi.org/10.3390/vaccines9101166
14. S. J. Russell, K. W. Peng, J. C. Bell, Oncolytic virotherapy, *Nat. Biotechnol.*, **30** (2012), 658–670. https://doi.org/10.1038/nbt.2287
15. P. Ambegoda, S. R. J. Jang, Resistance in oncolytic viral therapy for solid tumors, *Appl. Math. Comput.*, **469** (2024), 128546. https://doi.org/10.1016/j.amc.2024.128546

16. K. J. Mahasa, A. Eladdadi, L. de Pillis, R. Ouifki, Oncolytic potency and reduced virus tumor specificity in oncolytic virotherapy. A mathematical modelling approach, *PLoS One*, **12** (2017), e0184347. https://doi.org/10.1371/journal.pone.0184347

17. R. Vithanage, H. C. Wei, S. R. J. Jang, Bistability in a model of tumor-immune system interactions with an oncolytic viral therapy, *Math. Biosci. Eng.*, **19** (2022), 1559–1587. https://doi.org/10.3934/mbe.2022072

18. R. Vithanage, H. C. Wei, S. R. J. Jang, The Role of tumor activation and inhibition with saturation effects in a mathematical model of tumor and immune system interactions undergoing oncolytic viral therapy, *Math. Meth. Appl. Sci.*, **46** (2023), 10787–10813. https://doi.org/10.1002/mma.9152

19. R. Eftimie, G. Eftimie, Tumour-associated macrophages and oncolytic virotherapies: amathematical investigation into a complex dynamics, *Lett. Biomath.*, **5** (2018), S6–S35. https://doi.org/10.30707/LiB5.2Eftimiea

20. P. Cordelier, M. Costa, J. Fehrenbach, Slow-fast model and therapy optimization for oncolytic treatment of tumors, *Bull. Math. Biol.*, **84** (2022), 64. https://doi.org/10.1007/s11538-022-01025-3

21. K. Murphy, C. Weaver, L. J. Berg, *Janeway's Immunobiology*, 10^{th} edition, Garland Science, 2022.

22. K. M. Storey, E. L. Sean, T. L. Jackson, Modeling oncolytic viral therapy, immune checkpoint inhibition, and the complex dynamics of innate and adaptive immunity in glioblastoma treatment, *Front. Physiol.*, **11** (2020), 151. https://doi.org/10.3389/fphys.2020.00151

23. S. A. Felt, G. N. Droby, V. Z. Grdzelishvili, Ruxolitinib and polycation combination treatment overcomes multiple mechanisms of resistance of pancreatic cancer cells to oncolytic vesicular stomatitis virus, *J. Virol.*, **91** (2017), e00461–17. https://doi.org/10.1128/JVI.00461-17

24. L. J. S. Allen, *An Introduction to Mathematical Biology*, Pearson/Prentice Hall, 2007.

25. J. Hale, *Theory of Functional Differential Equations*, Springer, 1977.

26. Y. Kuang, *Delay Differential Equations: With Applications in Population Dynamics*, Academic Press, 2012.

27. H. L. Smith,*An Introduction to Delay Differential Equations with Applications to the Life Sciences*, Springer, 2011.

28. T. Koujima, H. Tazawa, T. Ieda, H. Araki, T. Fushimi, R. Shoji, et al., Oncolytic virus-mediated targeting of the ERK signaling pathway inhibits invasive propensity in human pancreatic cancer, *Mol. Ther. Oncolytics*, **17** (2020), 107–117. https://doi.org/10.1016/j.omto.2020.03.016

29. C. E. Engeland, C. Grossardt, R. Veinalde, S. Bossow, D. Lutz, J. K. Kaufmann, et al., CTLA-4 and PD-L1 checkpoint blockade enhances oncolytic measles virus therapy, *Mol. Ther.*, **22** (2014), 1949–1959. https://doi.org/10.1038/mt.2014.160

30. H. R. Thieme, Convergence results and a Poincare-Bendixson trichotomy for asymptotically autonomous differential equations,*J. Math. Biol.*, **30** (1992), 755–763.

31. A. Haseley, C. Alvarez-Breckenridge, A. R. Chaudhury, B. Kaur, Advances in oncolytic virus therapy for glioma, *Recent Pat. CNS. Drug Discov.*, **4** (2009), 1–13. https://doi.org/10.2174/157488909787002573

32. S. Meerani, Y. Yao, Oncolytic viruses in cancer therapy, *Eur. J. Sci. Res.*, **40** (2010), 156–171.

33. A. Rasa, P. Alberts, Oncolytic virus preclinical toxicology studies, *J. Appl. Toxicol.*, **43** (2023), 620–648. https://doi.org/10.1002/jat.4408

34. K. James, E. Eisenhauer, M. Christian, M. Terenziani, D. Vena, A. Muldal, et al., Measuring response in solid tumors: unidimensional versus bidimensional measurement,*J. Natl. Cancer Inst.*, **91** (1999), 523–528. https://doi.org/10.1093/jnci/91.6.523

35. V. Naumenko, J. Rajwani, M. Turk et al., Repeated dosing improves oncolytic rhabdovirus therapy in mice via interactions with intravascular monocytes, Commun. Biol., 5 (2022), 1385. https://doi.org/10.1038/s42003-022-04254-3

36. V. A. Kuznetsov, I. A. Makalkin, N. A. Taylor, A. S. Perelson,Nonlinear dynamics of immunogenic tumors: parameter estimation and global bifurcation analysis, *Bull. Math. Biol*, **56** (1994), 295–321. https://doi.org/10.1007/BF02460644

37. L. de Pillis, A. Radunskaya, C. Wiseman,A validated mathematical model of cell-mediated immune response to tumor growth, *Cancer Res.*, **65** (2005), 7950–7958. https://doi.org/10.1158/0008-5472.CAN-05-0564

38. R. Eftimie, J. Dushoff, B. W. Bridle, J. L. Bramson, D. J. D. Earn, Multi-stability and multi-instability phenomena in a mathematical model of tumor-immune-virus interactions,*Bull. Math. Biol.*, **73** (2011), 2932–2961. https://doi.org/10.1007/s11538-011-9653-5

39. M. R. Duran, A. Podolski-Reni, A. lvarez-Arenas, J. Dini, J. Belmonte-Beitia, M. Pesi, et al., Transfer of drug resistance characteristics between cancer cell subpopulations: a study using simple mathematical models, *Bull. Math. Biol.*, **78** (2016), 1218–1237. https://doi.org/10.1007/s11538-016-0182-0

40. C. Macnamara, R. Eftimie,Memory versus effector immune responses in oncolytic virotherapies, *J. Theor. Biol.*, **377** (2015), 1–9. https://doi.org/10.1016/j.jtbi.2015.04.004

41. N. Komarova, D. Wodarz, *Targeted Cancer Treatment in Silico: Small Molecule Inhibitors and Oncolytic Viruses*, Birkhauser, Switzerland, 2013.

42. B. Pulendran, J. Z. Oh, H. I. Nakaya, R. Ravindran, D. A. Kazmin, Immunity to viruses: learning from successful human vaccines, *Immunol. Rev.*, **255** (2013), 243–255. https://doi.org/10.1111/imr.12099

43. Z. Pancer, M. D. Cooper, The evolution of adaptive immunity, *Annu. Rev. Immunol.*, **24** (2006), 497–518. https://doi.org/10.1146/annurev.immunol.24.021605.090542

44. S. Marino, I. B. Hogue, C. J. Ray, D. E. Kirschner, A methodology for performing global uncertainty and sensitivity analysis in systems biology, *J. Theor. Biol.*, **254** (2008), 178–196. https://doi.org/10.1016/j.jtbi.2008.04.011

45. T. C. Liu, E. Galanis, D. Kirn, Clinical trial results with oncolytic virotherapy: a century of promise, a decade of progress, *Nat. Clin. Pract. Oncol.*, **4** (2007), 101–117. https://doi.org/10.1038/ncponc0736

46. A. De Matos, L. S. Franco, G. McFadden, Oncolytic viruses and the immune system: the dynamic duo, *Mol. Ther. Methods Clin. Dev.*, **17** (2020), 349–358. https://doi.org/10.1016/j.omtm.2020.01.001

47. C. J. Breitbach, Targeted inflammation during oncolytic virus therapy severely compromises tumor blood flow, *Mol. Ther.*, **15** (2007), 1686–1693. https://doi.org/10.1038/sj.mt.6300215
48. M. C. Speranza, K. Kasai, S. E. Lawler, Preclinical mouse models for analysis of the therapeutic potential of engineered oncolytic herpes viruses, *ILAR J.* **1** (2016), 63–72. https://doi.org/10.1093/ilar/ilw002
49. M. Kozak, What is strong correlation?, *Teach. Stat.*, **31** (2009), 85–86. https://doi.org/10.1111/j.1467-9639.2009.00387.x
50. L. Sun, Y. Su, A. Jiao, X. Wang, B. Zhang, T cells in health and disease, *Signal Transduct. Target. Ther.*, **8** (2023), 235. https://doi.org/10.1038/s41392-023-01471-y
51. D. F. Hale, T. J. Vreeland, G. E. Peoples, Arming the immune system through vaccination to prevent cancer recurrence, *Am. Soc. Clin. Oncol. Educ. Book*, **36** (2016), e159–e167. https://doi.org/10.1200/EDBK_158946
52. H. C. Wei, Numerical revisit to a class of one-predator, two-prey models, *Int. J. Bifurcation Chaos*, **20** (2010), 2521–2536. https://doi.org/10.1142/S0218127410027143
53. H. C. Wei, The dynamics of the Luo-Rudy model, *Int. J. Bifurcation Chaos*, **20** (2010), 4055–4066. https://doi.org/10.1142/S0218127410028185
54. M. H. Andersen, D. Schrama, P. Straten, J. C. Becker, Cytotoxic T cells, *J. Invest. Dermatol.*, **126** (2006), 32–41. https://doi.org/10.1038/sj.jid.5700001
55. C. M. Rollings, L. V. Sinclair, H. J. M. Brady, D. A. Cantrell, S. H. Ross, Interleukin-2 shapes the cytotoxic T cell proteome and immune environment-sensing programs, *Sci. Signal.*, **11** (2018), eaap8112. https://doi.org/10.1126/scisignal.aap8112
56. S. Banerjee, S. Khajanchi, S. Chaudhuri, A mathematical model to elucidate brain tumor abrogation by immunotherapy with T11 target structure, *PLoS One*, **10** (2015), e0123611. https://doi.org/10.1371/journal.pone.0123611
57. P. A. Abrams, Adaptive foraging by predators as a cause of predator-prey cycles, *Evol. Ecol.*, **6** (1992), 56–72. https://doi.org/10.1007/BF02285334
58. A. Y. Morozov, Incorporating complex foraging of zooplankton in models: role of micro-and mesoscale processes in macroscale patterns, in *Dispersal, Individual Movement and Spatial Ecology: A Mathematical Perspective*, Springer, New York, (2013), 1–10.
59. H. C. Wei, A mathematical model of intraguild predation with prey switching, *Math. Comput. Simul.*, **165** (2019), 107–118. https://doi.org/10.1016/j.matcom.2019.03.004
60. S. Ruan, Absolute stability, conditional stability and bifurcation in Kolmogorov-type predator-prey systems with discrete delays, *Quart. Appl. Math.*, **59** (2001), 159–173. https://doi.org/10.1090/qam/1811101
61. J. A. Nelder, R. Mead, A simplex method for function minimization, *Comput. J.*, **7** (1965), 308–313. https://doi.org/10.1093/comjnl/7.4.308
62. X. Fu, L. Tao, X. Zhang, Genetically coating oncolytic herpes simplex virus with CD47 allows efficient systemic delivery and prolongs virus persistence at tumor site, *Oncotarget*, **9** (2018), 34543–34553. https://doi.org/10.18632/oncotarget.26167

63. I. Kareva, K. A. Luddy, C. O'Farrelly, R. A. Gatenby, J. S. Brown, Predator-prey in tumor-immune interactions: A wrong model or just an incomplete one?, *Front. Immunol.*, **12** (2021), 668221. https://doi.org/10.3389/fimmu.2021.668221

64. H. Fukuhara, Y. Ino, T. Todo, Oncolytic virus therapy: a new era of cancer treatment at dawn, *Cancer Sci.*, **107** (2016), 1373–1379. https://doi.org/10.1111/cas.13027

65. Z. S. Guo, Z. Liu, S. Kowalsky, M. Feist, P. Kalinski, B. Lu, et al., Oncolytic immunotherapy: conceptual evolution, current strategies, and future perspectives, *Front. Immunol.*, **8** (2017), 1–15. https://doi.org/10.3389/fimmu.2017.00555

66. L. Aurelian, Oncolytic viruses as immunotherapy: progress and remaining challenges, *OncoTargets Ther.*, **9** (2016), 2627–2637. https://doi.org/10.2147/OTT.S63049

67. S. Guedan, R. Alemany, CAR-T cells and oncolytic viruses: joining forces to overcome the solid tumor challenge, *Front. Immunol.*, **89** (2018), 1–10. https://doi.org/10.3389/fimmu.2018.02460

68. R. Mohanty, C. R. Chowdhury, S. Arega, P. Sen, P. Ganguly, N. Ganguly, CAR T cell therapy: A new era for cancer treatment, *Oncol. Rep.*, **42** (2019), 2183–2195. https://doi.org/10.3892/or.2019.7335

69. S. Feins, W. Kong, E. F. Williams, M. C. Milone, J. A. Fraietta, An introduction to chimeric antigen receptor (CAR) T-cell immunotherapy for human cancer, *Am. J. Hematol.*, **94** (2019), S3–S9. https://doi.org/10.1002/ajh.25418

70. A. Turdo, C. M. Cristiani, N. Schaft, CAR T-cells: novel therapeutic approaches in the new era of cancer immunotherapy, *Front. Mol. Med.*, **3** (2023), 1239013. https://doi.org/10.3389/fmmed.2023.1239013

71. M. Al-Haideri, S. B. Tondok, S. H. Safa, A. H. maleki, S. Rostami, A. T. Jalil, et al., CAR-T cell combination therapy: the next revolution in cancer treatment, *Cancer Cell Int.*, **22** (2022). https://doi.org/10.1186/s12935-022-02778-6

72. A. M. Malfitano, S. D. Somma, C. A. Iannuzzi, F. Pentimalli, G. Portella, Virotherapy: From single agents to combinatorial treatments, *Biochem. Pharmacol.*, **177** (2020), 113986. https://doi.org/10.1016/j.bcp.2020.113986

73. I. Gruber, N. Landenberger, A. Staebler, M. Hahn, D. Wallwiener, T. Fehm, Relationship between circulating tumor cells and peripheral T-cells in patients with primary breast cancer, *Anticancer Res.*, **33** (2013), 2233–2238.

74. A. Rotte, M. J. Frigault, A. Ansari, B. Gliner, Dose-response correlation for CAR-T cells: a systematic review of clinical studies, *J. Immunother. Cancer*, **10** (2022). https://doi.org/10.1136/jitc-2022-005678

75. M. Frigault, A. Rotte, A. Ansari, B. Gliner, C. Heery, Dose fractionation of CAR-T cells. A systematic review of clinical outcomes, *J. Exp. Clin. Cancer Res.*, **42** (2023). https://doi.org/10.1186/s13046-022-02540-w

76. M. G. McCartney, Total blood and corpuscular volume in turkey hens, *Poult. Sci.*, **31** (1952), 184–185. https://doi.org/10.3382/ps.0310184

77. Z. Z. Zhang, T. Wang, X. F. Wang, Y. Q. Zhang, Improving the ability of CAR-T cells to hit solid tumors: Challenges and strategies, *Pharmacol. Res.*, **175** (2022). https://doi.org/10.1016/j.phrs.2021.106036

78. R. Bhat, J. Rommelaere, Emerging role of Natural killer cells in oncolytic virotherapy, *ImmunoTargets Ther.*, **4** (2015), 65–77. https://doi.org/10.2147/ITT.S55549

79. H. Wu, Y. Y. Deng, L. Liu, Q. H. Tan, C. H. Wang, M. M. Guo, et al., Intestinal ischemia-reperfusion of macaques triggers a strong innate immune response, *World J Gastroenterol.*, **20** (2014), 15327. https://doi.org/10.3748/wjg.v20.i41.15327

80. J. B. Swann, M. J. Smyth, Immune surveillance of tumors, *J. Clin. Invest.*, **117** (2007), 1137–1146. https://doi.org/10.1172/JCI31405

81. A. Eldar-Boock, D. Polyak, A. Scomparin, R. Satchi-Fainaro, Nano-sized polymers and liposomes designed to deliver combination therapy for cancer, *Curr. Opin. Biotechnol.*, **24** (2013), 682–689. https://doi.org/10.1016/j.copbio.2013.04.014

82. W. Ratajczak, P. Niedźwiedzka-Rystwej, B. Tokarz-Deptula, W.Deptula, Immunological memory cells, *Cent. Eur. J. Immunol.*, **43** (2018), 194–203. https://doi.org/10.5114/ceji.2018.77390

83. D. H. Raulet, Interplay of natural killer cells and their receptors with the adaptive immune response, *Nat. Immunol.*, **5** (2004), 996–1002. https://doi.org/10.1038/ni1114

84. M. J. D. Esmatabadi, B. Bakhshinejad, F. M. Motlagh, S. Babashah, M. Sadeghizadeh, Therapeutic resistance and cancer recurrence mechanisms: Unfolding the story of tumor coming back, *J. Biosci.*, **41** (2016), 497–506. https://doi.org/10.1007/s12038-016-9624-y

85. E. Binz, U. M. Lauer, Chemovirotherapy: Combining chemotherapeutic treatment with oncolytic virotherapy, *Oncolytic Virother.*, **4** (2015), 39–48. https://doi.org/10.2147/OV.S54780

86. H. M. Nguyen, P. K. Bommareddy, A. W. Silk, D. Daha, Optimal timing of PD-1 blockade in combination with oncolytic virus therapy, *Semin. Cancer Biol.*, **86** (2022), 971–980. https://doi.org/10.1016/j.semcancer.2021.05.019

87. L. Aurelian, Oncolytic virotherapy: The questions and the promise, *Oncolytic Virother.* **2**, (2013), 19–29. https://doi.org/10.2147/OV.S39609

88. M. P. F. Damen, J.van Rheenen, C. L. G. J. Scheele, Targeting dormant tumor cells to prevent cancer recurrence, *FEBS J.*, **288** (2021), 6286–6330. https://doi.org/10.1111/febs.15626

Appendix

A. Special cases of ODE models

The ODE models of the special cases $d = 0$ and no resistant cancer cells are briefly discussed in this appendix.

A.1. The case of $d = 0$

Since $d = 0$, it follows that $(\hat{T}_s, \hat{T}_r, 0, 0, 0) = (0, K, 0, 0, 0)$. If the maximal immune cell proliferation rate $\dfrac{\alpha K}{m + K}$ is greater than its death rate γ, then the interaction is able to support another equilibrium, $E_2^0 = (0, \xi, 0, 0, \tilde{Z}^0)$, where

$$\xi = \frac{m\gamma}{\alpha - \gamma} \text{ and } \tilde{Z}^0 = \frac{r_r(1 - \xi/K)}{k_r}. \tag{A.1}$$

It can be verified that E_2^0 is asymptotically stable if

$$(r_s - r_r\frac{k_s}{k_r})(1 - \frac{\xi}{K}) - a < 0, \tag{A.2}$$

and unstable if the above inequality is reversed. Moreover, if

$$\alpha > \gamma, \quad (1 - \frac{\xi}{K})(r_s - r_r\frac{k_s}{k_r}) > a, \tag{A.3}$$

then the model (2.1) with $\tau = 0$ and $d = 0$ has an equilibrium of the form $E_3^0 = (\bar{T}_s^0, \bar{T}_r^0, 0, 0, \bar{Z}^0)$, where

$$\begin{aligned}
\bar{T}_s^0 &= \zeta - \frac{a\zeta}{a + \left(1 - \frac{\zeta}{K}\right)\left(\frac{k_r r_s}{k_s} - r_r\right) - \frac{ak_r}{k_s}}, \\
\bar{T}_r^0 &= \frac{a\zeta}{a + \left(1 - \frac{\zeta}{K}\right)\left(\frac{k_r r_s}{k_s} - r_r\right) - \frac{ak_r}{k_s}}, \\
\bar{Z}^0 &= \frac{1}{k_s}\left(r_s\left(1 - \frac{\zeta}{K}\right) - a\right).
\end{aligned} \tag{A.4}$$

Observe that the last inequality in (A.3) implies

$$(r_s - r_r\frac{k_s}{k_r})(1 - \frac{\xi}{K}) - a > 0.$$

Therefore, the existence of E_3^0 implies that E_2^0 is unstable. The Jacobian matrix at E_3^0 has the same entries as $J(E_2)$ defined in (3.14). We can conclude that E_3^0 is asymptotically stable if (3.11) and (3.16) are satisfied with d being replaced by 0. The existence and stability of boundary equilibria of (2.1) with $\tau = 0$ and $d = 0$ are summarized in Table A1.

Table A1. The existence and stability conditions of boundary equilibria of system (2.1) with $\tau = 0$ and $d = 0$. The asterisk * represents the substitution of $\bar{T}_s, \bar{T}_r, \bar{Z}$ in (3.11) and (3.16) with $\bar{T}_s^0$, $\bar{T}_r^0$ and $\bar{Z}^0$, respectively. The stability column provides sufficient conditions for the asymptotic stability of the corresponding equilibrium.

Boundary equilibrium (T_s, T_r, T_i, V, Z)	Existence	Stability
$E_0 = (0, 0, 0, 0, 0)$	Always	Unstable
$E_1^0 = (0, K, 0, 0, 0)$	Always	$\frac{\alpha K}{m + K} < \gamma$
$E_2^0 = (0, \xi, 0, 0, \tilde{Z}^0)$	$\frac{\alpha K}{m + K} > \gamma$	(A.2)
$E_3^0 = (\bar{T}_s^0, \bar{T}_r^0, 0, 0, \bar{Z}^0)$	(A.3)	(3.11)* & (3.16)*

Comparing Table A1 with Table 1, it is observed that $E_1^0 = E_1$ when $d = 0$, as in this instance $\hat{T}_s = 0$. Therefore, the condition $c > \beta q\hat{T}_s$ given in Table 1 is trivially true and the stability of E_1^0 in Table A1

reduces to $\frac{\alpha K}{m+K} < \gamma$ only. Further, the second inequality in (A.3) implies $\xi < K$, i.e., $\frac{\alpha K}{m+K} > \gamma$. Thus, the equilibrium E_3^0 given in Table A1 is the equilibrium E_2 given in Table 1, and therefore the stability of E_3^0 is based on E_2. The existence of E_3 in Table 1 requires that $c < \beta q \hat{T}_s$, which is impossible in the case $d = 0$, and there is no such corresponding equilibrium in Table A1.

Parallel to Theorem 3.1, we can also derive sufficient conditions for the global stability of E_1^0 as follows, without providing a proof.

Theorem A.1. *Let $\tau = 0$ and $d = 0$. The equilibrium $E_1^0 = (0, K, 0, 0, 0)$ is globally asymptotically stable in D for (2.1) if $\frac{\alpha K}{m+K} < \gamma$ and $c > \beta q K$.*

A.2. The scenario of no resistant tumor cells

Assume that there are no resistant tumor cells initially, $T_r(0) = 0$, and no mutation, $a = 0$. Then, $T_r(t) = 0$ for all $t > 0$, and model (2.1) with $\tau = 0$ becomes a four-dimensional system involving only T_s, T_i, V, and Z. If, in addition, there are no infected tumor cells and viruses initially, $T_i(0) = 0 = V(0)$, then $T_i(t) = 0 = V(t)$ for all $t > 0$, and we obtain the following two-dimensional system:

$$\begin{aligned} T_s'(t) &= r_s T_s(t)\Big(1 - \frac{T_s(t)}{K}\Big) - k_s T_s(t) Z(t) \\ Z'(t) &= \frac{\alpha T_s(t) Z(t)}{m + T_s(t)} - \gamma Z(t). \end{aligned} \tag{A.5}$$

The system (A.5) has three equilibria, where $(0, 0)$ and $(K, 0)$ always exist, and $(\xi, \tilde{Z})$ is biologically feasible only if $\frac{\alpha K}{m+K} > \gamma$, with $\xi = \frac{\gamma m}{\alpha - \gamma}$ defined in (3.5) and

$$\tilde{Z} = \frac{r_s}{k_s}(1 - \frac{\xi}{K}). \tag{A.6}$$

It is straightforward to see that $(0, 0)$ is always unstable, while $(K, 0)$ is asymptotically stable if $\frac{\alpha K}{m+K} < \gamma$ and unstable if $\frac{\alpha K}{m+K} > \gamma$. We assume $\frac{\alpha K}{m+K} > \gamma$ so that $(\xi, \tilde{Z})$ exists. It follows from the Dulac criterion [24] that (A.5) has no positive periodic solutions, which implies that $(\xi, \tilde{Z})$ is globally asymptotically stable in $\mathring{\mathbb{R}}^2_+$ for the two-dimensional model (A.5) by the Poincaré-Bendixson Theorem [24]. As a result, we see that $\tilde{E}_2 = (\xi, 0, 0, \tilde{Z})$ is asymptotically stable if

$$(b + k_i \tilde{Z})(c + k_v \tilde{Z}) > qb\beta\xi. \tag{A.7}$$

Let $c < \beta q K$ so that $\tilde{E}_3 = (\tilde{T}_s, \tilde{T}_i, \tilde{V}, 0)$ exists, where

$$\tilde{T}_s = \frac{c}{\beta q}, \quad \tilde{V}_0 = \frac{r_s}{\beta}(1 - \frac{\tilde{T}_s}{K}), \quad \tilde{T}_i = \frac{c}{qb}\tilde{V}. \tag{A.8}$$

See Section 3.3 of [15]. Applying the Routh-Hurwitz criterion [24], without delving into all the details, $\tilde{E}_3$ is locally asymptotically stable if it satisfies the following conditions

$$\frac{\alpha(\tilde{T}_s + \tilde{T}_i)}{m + \tilde{T}_s + \tilde{T}_i} < \gamma \text{ and } \frac{r_s(b + c)}{K}(b + c + \frac{r_s \tilde{T}_s}{K}) - \beta^2 qb\tilde{V} > 0. \tag{A.9}$$

The above results are summarized in the following table.

Table A2. Existence and stability conditions of boundary equilibria of system (2.1) of no resistant tumor cells. The stability column provides sufficient conditions for the asymptotic stability of the corresponding equilibrium.

Boundary equilibrium (T_s, T_i, V, Z)	Existence	Stability
$E_0 = (0, 0, 0, 0)$	Always	Unstable
$\tilde{E}_1 = (K, 0, 0, 0)$	Always	$\beta qK < c$ and $\dfrac{\alpha K}{m+K} < \gamma$
$\tilde{E}_2 = (\xi, 0, 0, \tilde{Z})$	$\dfrac{\alpha K}{m+K} > \gamma$	(A.7)
$\tilde{E}_3 = (\tilde{T}_s, \tilde{T}_i, \tilde{V}, 0)$	$\beta qK > c$	(A.9)

Parallel to Theorem 3.1, we can also derive sufficient conditions for the global stability of $\tilde{E}_1$ as follows, without providing a proof.

Theorem A.2. *Let $\tau = 0$, $a = 0$, and $T_r(0) = 0$. The equilibrium $\tilde{E}_1 = (K, 0, 0, 0)$ is globally asymptotically stable in $\{(T_s, T_i, V, Z) \in \mathbb{R}^4_+ : T_s > 0\}$ if $\dfrac{\alpha K}{m+K} < \gamma$ and $c > \beta qK$.*

Notice the stability of $\tilde{E}_2$ given in Table A2, (A.7), is the stability condition (3.16) for E_2 in Table 1, while the other condition (3.11) is trivially true for the case of no resistant tumor cells $a = 0$ and $T_r \equiv 0$. In addition, the equilibrium $\tilde{E}_1$ in Table A2 corresponds to the equilibrium point $E_1 = (\hat{T}_s, \hat{T}_r, 0, 0, 0)$ in Table 1 with $T_r \equiv 0$, and they have the same existence condition. In addition, the inequalities (3.20) are equivalent to those given in (A.9), and therefore both equilibria have the same stability conditions.

B. Special cases of DDE models

B.1. The case of $d = 0$

The resulting model always has equilibria $E_0 = (0, 0, 0, 0, 0)$, and $E_1^0 = (0, K, 0, 0, 0)$. Similar to Section 4.2, it can be seen that E_0 is always unstable for $\tau \geq 0$ and E_1 is asymptotically stable for $\tau \geq 0$ if $\dfrac{\alpha K}{m+K} < \gamma$, and unstable for $\tau \geq 0$ if $\dfrac{\alpha K}{m+K} > \gamma$.

Let $\dfrac{\alpha K}{m+K} > \gamma$. Then, $E_2^0 = (0, \xi, 0, 0, \tilde{Z}^0)$ exits, where $\xi = \dfrac{m\gamma}{\alpha - \gamma}$, and $\tilde{Z}^0 = \dfrac{r_r}{k_r}(1 - \dfrac{\xi}{K})$. It can be argued that E_2^0 is asymptotically stable for $\tau \geq 0$ if certain conditions on the parameters are met. On the other hand, under certain constraints on the parameters, there exists a critical delay τ_c beyond which E_2^0 becomes unstable as τ increases. Indeed, let

$$p_1 = (\frac{r_r\zeta}{K} + \gamma), \quad p_2 = \frac{\gamma r_r \xi}{K}, \quad q_1 = -\gamma, \quad q_2 = \frac{\gamma m k_r \tilde{Z}^0}{m+\xi} - \frac{\gamma r_r \xi}{K}.$$

We summarize the following without proof as the proof is similar to that given previously.

Theorem B.1. *Let* $d = 0$, $\dfrac{\alpha K}{m+K} > \gamma$, $a_{11} < 0$, *and* $p_2 - q_2 < 0$. *Then, there exists* $\tau_0 > 0$ *such that* E_2^0 *is asymptotically stable for* $\tau \in [0, \tau_0)$ *and* $\dfrac{d(Re\lambda)}{d\tau}\Big|_{\tau=\tau_0} > 0$.

Assume (A.3) so that $E_3^0 = (\bar{T}_s^0, \bar{T}_r^0, 0, 0, \bar{Z}^0)$ exists. Suppose that (3.11) and (3.16) are satisfied with $d = 0$, i.e., E_3^0 is asymptotically stable for the ODE model with $d = 0$. Then, one can also find a critical delay τ_c such that E_3^0 is asymptotically stable for $\tau \in [0, \tau_c)$, and the transversality condition for λ can also be verified. We do not present the results here since the proof and conclusion are similar.

B.2. The scenario of no resistant tumor cells

The proof of the following proposition is routine and is omitted.

Proposition B.1. *The following is true for system* (2.1) *with* $a = 0$ *and* $T_r(0) = 0$.

(a) $E_0 = (0, 0, 0, 0)$ *is unstable for* $\tau \geq 0$.

(b) $\tilde{E}_1 = (K, 0, 0, 0)$ *is asymptotically stable for* $\tau \geq 0$ *if* $c > \beta q K$ *and* $\dfrac{\alpha K}{m+K} < \gamma$, *and unstable if either* $c < \beta q K$ *or* $\dfrac{\alpha K}{m+K} > \gamma$.

Let

$$\tilde{p}_1^2 - \tilde{q}_1^2 - 2\tilde{p}_2 = \Big(\frac{r_s\zeta}{K}\Big)^2, \quad \tilde{p}_2 + \tilde{q}_2 = \frac{k_s m\tilde{Z}\gamma}{m+\zeta},$$

$$\tilde{p}_2 - \tilde{q}_2 = \frac{2r_s\zeta\gamma}{K} - \frac{k_s m\tilde{Z}\gamma}{m+\zeta}.$$

The delay τ can affect the stability of $\tilde{E}_2$ as illustrated below.

Theorem B.2. *Let* $\dfrac{\alpha K}{m+K} > \gamma$. *Then,* $\tilde{E}_2 = (\zeta, 0, 0, \tilde{Z})$ *exists, and*

(a) $\tilde{E}_2$ *is asymptotically stable for* $\tau \geq 0$ *if* $(k_i\tilde{Z} + b)(k_v\tilde{Z} + c) > qb\beta\zeta$ *and* $\tilde{p}_2 - \tilde{q}_2 > 0$.

(b) If $(k_i\tilde{Z} + b)(k_v\tilde{Z} + c) < qb\beta\zeta$ *or* $\tilde{p}_2 - \tilde{q}_2 < 0$, *then there exists* $\tau_0 > 0$ *such that* $\tilde{E}_2$ *is asymptotically stable for* $\tau \in [0, \tau_0)$ *and* $\dfrac{d(Re\lambda)}{d\tau}\Big|_{\tau=\tau_0} \neq 0$.

C. Proofs of mathematical results

Proof of Theorem 2.1. Since f and $\dfrac{\partial f}{\partial X}$ exist and are continuous on $\mathbb{R}^5_+ \times \mathbb{R}^5_+$, (2.1) has a unique solution on $[-\tau, t_0)$ for some $t_0 > 0$. Moreover, if $X, Y \geq 0$ with $x_j = 0$, then $f_j(X, Y) \geq 0$, and thus solutions remain nonnegative on $[-\tau, t_0)$ by [27].

As

$$T_s'(t) + T_r'(t) \leq (r_s T_s(t) + r_r T_r(t))(1 - \frac{T_s(t) + T_r(t)}{K})$$

and

$$T_s(0) + T_r(0) \leq K,$$

we have $T_s(t) + T_r(t) \le K$ on $[0, t_0)$. Next,

$$T_s'(t)+T_r'(t)+T_i'(t) \le (r_sT_s(t)+r_rT_r(t))(2-\frac{T_s(t)+T_r(t)}{K})-r_sT_s(t)-r_rT_r(t)-bT_i(t) \le C_1-b_1(T_s(t)+T_r(t)+T_i(t))$$

on $[0, t_0)$ for some $C_1 > 0$ and $b_1 = \min\{r_s, r_r, b\} > 0$. It follows that $T_i(t) \le \hat{C}_1$ for $0 \le t < t_0$ for some $\hat{C}_1 > 0$. Then, $V'(t) \le qb\hat{C}_1 - cV$, and we have $V(t) \le C_2$ on $[0, t_0)$ for some $C_2 > 0$.

Notice

$$Z'(t) \le \frac{\alpha}{m}\Big(T_s(t-\tau) + T_r(t-\tau) + T_i(t-\tau)\Big)Z(t-\tau) - \gamma Z(t).$$

Let

$$M(t) = T_s(t-\tau) + T_r(t-\tau) + T_i(t-\tau) + V(t-\tau) + Z(t).$$

Then, by the given assumption,

$$\begin{aligned} M'(t) &\le [r_sT_s(t-\tau) + r_rT_r(t-\tau)]\Big(2 - \frac{T_s(t-\tau)+T_r(t-\tau)}{K}\Big) + qbT_i(t-\tau) - r_sT_s(t-\tau) \\ &-r_rT_r(t-\tau) - bT_i(t-\tau) - cV(t-\tau) - \gamma Z(t) \\ &\le \hat{M} - \hat{\gamma}M(t) \end{aligned}$$

on $[0, t_0)$ for some $\hat{M} > 0$, and

$$\hat{\gamma} = \min\{r_s, r_r, b, c, \gamma\} > 0.$$

Hence, $M(t)$ is bounded on $[0, t_0)$, and solutions cannot blow up as $t \uparrow t_0$. Therefore, solutions exist on $[0, \infty)$ and remain nonnegative. Similar arguments can be applied to show that solutions are bounded on $[0, \infty)$. ■

Proof of Proposition 3.1. Clearly, $(\hat{T}_s, \hat{T}_r, 0)$ is asymptotically stable, and

$$Z'(t) \le (\frac{\alpha K}{m+K} - \gamma)Z(t)$$

for all $t \ge 0$ implies $\lim_{t\to\infty} Z(t) = 0$ by the assumption. Thus, (3.1) is asymptotically autonomous [30] to the two-dimensional T_sT_r subsystem, under which $(\hat{T}_s, \hat{T}_r)$ is globally asymptotically stable in the region for which $T_s(0) + T_r(0) > 0$ by [15]. Therefore, $(\hat{T}_s, \hat{T}_r, 0)$ is globally asymptotically stable in Γ. ■

Proof of Theorem 3.1. By Proposition 3.4, $\lim_{t\to\infty} T_i(t) = 0 = \lim_{t\to\infty} V(t)$, and thus system (2.1) with $\tau = 0$ is asymptotically autonomous [30] to the three-dimensional model (3.1), where $(\hat{T}_s, \hat{T}_r, 0)$ is globally asymptotically stable in Γ by Proposition 3.1. Since $c > \beta qK > \beta q\hat{T}_s$ and $\frac{\alpha K}{m+K} < \gamma$, E_1 is asymptotically stable. It follows that E_1 is globally asymptotically stable in D. ■

Proof of Proposition 4.1. We only need to prove the second part of (b) for $\tau > 0$. Let

$$h(\lambda) = \frac{\alpha K}{m+K}e^{-\lambda\tau} - \gamma - \lambda$$

with $\tau > 0$. Then,

$$h(0) = \frac{\alpha K}{m+K} - \gamma > 0, \quad h'(\lambda) < 0$$

for $\lambda \geq 0$, and

$$h(\infty) = -\infty.$$

Therefore, $h(\lambda) = 0$ has one positive root, and hence $(\hat{T}_s, \hat{T}_r, 0)$ is unstable for all $\tau > 0$. ∎

Proof of Theorem 4.1 Suppose (4.9) has j positive roots x_n, $1 \leq j \leq 3$, each of which is simple. Then, (4.4) has j simple pure imaginary roots

$$\pm i\sqrt{x_n}, \quad 1 \leq n \leq j.$$

Clearly, for each n, $1 \leq n \leq j$, (4.10) and (4.11) have a unique solution $\omega_n\tau$ in $(0, 2\pi]$, $\omega_n = \sqrt{x_n}$. Let

$$\tau_n^l = \frac{1}{\omega_n}\left[\arccos\left(\frac{q_1\omega_n(\omega_n^3 - p_2\omega_n) + (p_1\omega_n^2 - p_3)(\gamma\omega_n^2 + q_2)}{(\gamma\omega_n^2 + q_2)^2 + q_1^2\omega_n^2}\right) + 2\pi l\right], \ 1 \leq n \leq j, \ l = 0, 1, 2, \ldots \quad \text{(C.1)}$$

if $\rho_s > 0$, and

$$\tau_n^l = \frac{1}{\omega_n}\left[2\pi - \arccos\left(\frac{q_1\omega_n(\omega_n^3 - p_2\omega_n) + (p_1\omega_n^2 - p_3)(\gamma\omega_n^2 + q_2)}{(\gamma\omega_n^2 + q_2)^2 + q_1^2\omega_n^2}\right) + 2\pi l\right], \ 1 \leq n \leq j, \ l = 0, 1, 2, \ldots \quad \text{(C.2)}$$

if $\rho_s \leq 0$. Define

$$\tau_0 = \min\{\tau_n^l : 1 \leq n \leq j, \ l = 0, 1, 2, \ldots\} = \tau_{n_0}^{l_0}, \quad \text{(C.3)}$$

and set $\omega_0 = \omega_{n_0}$. We verify the transversality condition at $\tau = \tau_0$, i.e., $\frac{dRe(\lambda)}{d\tau}|_{\tau=\tau_0} \neq 0$, by using

$$\text{Sign}\Big(\frac{dRe(\lambda)}{d\tau}\Big|_{\tau=\tau_0}\Big) = \text{Sign}\Big(Re(\frac{d\lambda}{d\tau})^{-1}\Big|_{\tau=\tau_0}\Big).$$

The transversality condition is a necessary condition for a Hopf bifurcation to occur [27].

Implicitly differentiate (4.4) with respect to τ, and we obtain

$$\left(\frac{d\lambda}{d\tau}\right)^{-1} = -\frac{\tau}{\lambda} + \frac{-2\gamma\lambda + q_1}{\lambda(-\gamma\lambda^2 + q_1\lambda + q_2)} - \frac{3\lambda^2 + 2p_1\lambda + p_2}{\lambda(\lambda^3 + p_1\lambda^2 + p_2\lambda + p_3)}.$$

It follows that

$$\Big(Re\left(\frac{d\lambda}{d\tau}\right)^{-1}|_{\tau=\tau_0}\Big) = \frac{-2\gamma^2\omega_0^2 - 2\gamma q_2 - q_1^2}{\gamma^2\omega_0^4 + 2\gamma q_2\omega_0 + q_1\omega_0^2 + q_2^2} + \frac{3\omega_0^4 + (2p_1^2 - 4p_2)\omega_0^2 - 2p_1p_3 + p_2^2}{\omega_0^6 + (p_1^2 - 2p_2)\omega_0^4 + (p_2^2 - 2p_1p_3)\omega_0^2 + p_3^2},$$

and by (4.8),

$$\omega_0^6 + (p_1^2 - 2p_2)\omega_0^4 + (p_2^2 - 2p_1p_3)\omega_0^2 + p_3^2 = \gamma^2\omega_0^4 + 2\gamma q_2\omega_0^2 + q_1^2\omega_0^2 + q_2^2.$$

As a result,

$$\Big(Re(\frac{d\lambda}{d\tau})^{-1}|_{\tau=\tau_0}\Big) = \frac{3\omega_0^4 + (2p_1^2 - 4p_2 - 2\gamma^2)\omega_0^2 - 2\gamma q_2 - q_1^2 - 2p_1p_3 + p_2^2}{\gamma^2\omega_0^4 + (2\gamma q_2 + q_1^2)\omega_0^2 + q_2^2}.$$

The denominator of the above expression is clearly positive, and the numerator is $F'(x_0)$, where $x_0 = \omega_0^2$ and F is defined in (4.9). Since x_0 is a simple root, $F'(x_0) \neq 0$, and the transversality condition is satisfied. ∎

AIMS Press

© 2024 the Author(s), licensee AIMS Press. This is an open access article distributed under the terms of the Creative Commons Attribution License (http://creativecommons.org/licenses/by/4.0)